ARTICLES
https://doi.org/10.1038/s41477-020-0630-6

nature plants

Rice pollen aperture formation is regulated by the interplay between OsINP1 and OsDAF1

Xu Zhang[1,4], Guochao Zhao[1,2,4], Qian Tan[1], Hui Yuan[1,2], Natalie Betts[3], Lu Zhu[1], Dabing Zhang[1,3] and Wanqi Liang[1]✉

The aperture on the pollen surface provides an exit for the emerging pollen tube. Apertures exhibit huge morphological variation across plant species—grasses, including rice, possess a complex aperture consisting of an annulus and an operculum—but little is known about how this species-specific cell-surface pattern forms. Here, we report a lectin receptor-like kinase in *Oryza sativa*, OsDAF1, which is essential for annulus formation and thus for fertility. OsDAF1 is evenly distributed in early microsporocytes but localizes to the distal pre-aperture site at the tetrad stage. We further reveal that the rice orthologue of a key aperture factor in *Arabidopsis*, OsINP1, has conserved and diversified roles in rice aperture formation. Disruption of OsINP1 prevents formation of the aperture, precluding pollen-tube germination. Furthermore, our results demonstrate that OsINP1 is required for polarization of OsDAF1 via direct protein interaction, suggesting that OsINP1 has an additional role in the formation of annulus that is absent in *Arabidopsis*. Our study reveals the importance of the aperture for rice grain yield and reveals mechanisms controlling pollen aperture development in cereal species.

Pollen provides an ideal model for studying cell-surface patterning and polarity, which is precisely controlled and differs characteristically between species. Each pollen grain is surrounded by two protective layers: an inner layer (intine) and a robust outer layer (exine, deposited on a base of primexine and further divided into sexine and nexine layers)[1,2]. The outer exine consists of a highly resistant lipid-rich component, sporopollenin, whose deposition is the key determinant of pollen surface patterning[3,4].

A major interspecies distinction of pollen is the size, shape, position and number of apertures. An aperture is a gap in exine deposition, critical for pollen germination, that permits water uptake during rehydration and provides an exit for the pollen tube[5,6]. During pollen development, microspore mother cells (MMCs) divide into a tetrad containing four microspores, each surrounded by a callose cell wall. Aperture formation is initiated soon after the completion of meiosis, and is completed during pollen maturation after release from the tetrad[7–10]. Different aperture patterns are related to different styles of meiotic cytokinesis, callose deposition and degradation, and microspore ploidy[11–15]; meanwhile, aperture number and shape are under heavy selective pressure[5,16,17]. In cereal pollen, the aperture is a single pore located at the distal polar site, encircled by a bulging ring-like annulus and covered by a cap-like operculum[18] (see Fig. 1a). The annulus is a raised and thickened border of exine and the operculum is an isolated area of exine supported by a layer termed Zwischenkörper[19].

Research into pollen aperture morphology has spanned more than a century, but genes directly involved in aperture formation have only recently been reported. In *Arabidopsis*, *INAPERTURATE POLLEN1* (*INP1*) was shown to be responsible for pollen aperture initiation and formation by keeping plasma membrane close to the callose wall, marking future aperture sites and preventing primexine formation and sporopollenin deposition[11,20–22]. More recently, D6 PROTEIN KINASE-LIKE3 (D6PKL3) in *Arabidopsis* has been shown to exhibit a similar protein subcellular location. Although no direct interaction was detected, D6PKL3 and INP1 could each affect the location of the other protein, and probably work together indirectly to facilitate the formation of apertures[23]. Whereas protein disruption led to the disappearance of all three *Arabidopsis* apertures, the pollen could germinate, in stark contrast to maize, in which inaperturate *ZmINP1* mutants were sterile[21]. Thus, study of aperture formation is critically important for understanding fertility in agriculturally important grass species, but the factors that direct the formation of these complex structures remain largely unknown.

Here, we report the isolation and characterisation of a rice (*O. sativa*) legume-lectin receptor-like kinase gene, *DEFECTIVE IN APERTURE FORMATION1* (*OsDAF1*), that is involved in aperture patterning formation. We demonstrate that loss of *OsDAF1* leads to disappearance of the annulus and complete male sterility, and that OsDAF1 protein localizes to future aperture sites in developing pollen. Furthermore, OsDAF1 co-locates and directly interacts with OsINP1. *OsINP1* mutation disrupts the polar localization of OsDAF1, causes disappearance of the entire aperture, and results in male sterility. Our results provide important insights into how surface patterning and polarity, and thus fertility, are controlled in developing cereal pollen.

Results

***osdaf1* mutants exhibit defective pollen apertures and are male sterile.** Previously, we isolated two completely sterile lines from our mutant library in *O. sativa* ssp. japonica 9522 (ref. [24]). Because of the defective aperture phenotypes described below, we named the two mutants *defective in aperture formation1-1* (*osdaf1-1*) and *osdaf1-2*. Both mutants exhibited normal vegetative development but relatively thin, pale anthers (Extended Data Fig. 1a–d). Transverse sections showed that mutant microspores developed normally until stage 11 (on the basis of the previous classification[25]), but

[1]Joint International Research Laboratory of Metabolic & Developmental Sciences, State Key Laboratory of Hybrid Rice, School of Life Sciences and Biotechnology, Shanghai Jiao Tong University, Shanghai, China. [2]Development Center of Plant Germplasm Resources, College of Life Sciences, Shanghai Normal University, Shanghai, China. [3]School of Agriculture, Food and Wine, University of Adelaide, Waite Campus, Glen Osmond, South Australia, Australia. [4]These authors contributed equally: Xu Zhang, Guochao Zhao. ✉e-mail: wqliang@sjtu.edu.cn

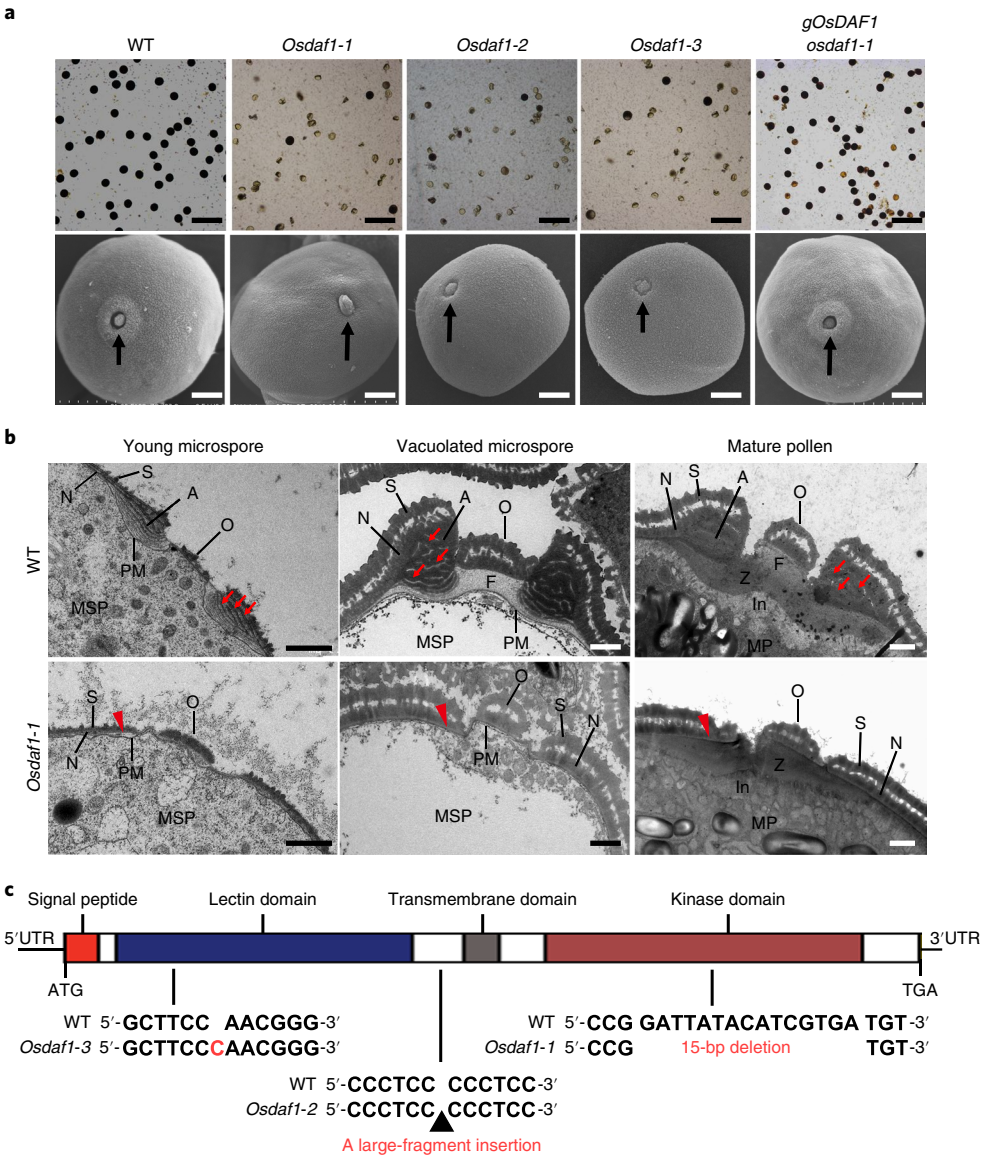

Fig. 1 | *OsDAF1* is required for rice aperture patterning. a, Comparison of mature pollen grains by I_2-KI staining (top) and SEM (bottom) for wild type (WT), *osdaf1-1*, *osdaf1-2* and *osdaf1-3* mutants, and the *osdaf1-1* mutant rescued by complementation with genomic *OsDAF1* sequence (*gOsDAF1 osdaf1-1*). Aborted pollen grains do not stain dark blue with iodine. Arrows indicate the annulus area. **b**, TEM observation of wild-type and *osdaf1-1* pollen aperture areas at the young microspore stage (left), vacuolated microspore stage (middle) and mature pollen stage (right). A, annulus; N, nexine; S, sexine; O, operculum; PM, plasma membrane; MSP, microspore; F, fibrillar-granular layer; Z, Zwischenkörper layer; In, intine; MP, mature pollen. Arrows indicate the trilamellated structures in annulus. Arrowheads indicate where the annulus structure is absent in *osdaf1-1* pollen. **c**, A schematic diagram of the *OsDAF1* gene. The putative domains of the OsDAF1 protein and the mutation sites of *osdaf1-1*, *osdaf1-2* and *osdaf1-3* are indicated. UTR, untranslated region. The phenotypes in **a**, **b** were observed at least three times independently with similar results. Scale bars: 100 μm (**a**, top), 5 μm (**a**, bottom) and 1 μm (**b**).

at the pollen maturation stage, most pollen grains were aborted (Fig. 1a and Extended Data Figs. 1f and 2). Surviving pollen grains lacked the annulus structure (Fig. 1a), which prevented pollen-tube germination both in vitro and in vivo (Extended Data Fig. 3), leading to complete male sterility (Extended Data Fig. 1e).

To investigate the *osdaf1* phenotype in detail, we examined transmission electron microscopy (TEM) sections of wild-type and *osdaf1-1* anthers at different stages. At tetrad stage after meiosis (stage 8b), we observed initiation of the aperture area, but there was no difference between the wild type and mutant (Extended Data Fig. 4a). After the release of young microspores from tetrads (stage 9), the operculum and annulus begin to develop. In the wild type, the plasma membrane at the annulus started to recede, and several darkly stained parallel trilamellated structures formed (indicated by red arrows, Fig. 1b and Extended Data Fig. 4b). In the mutant, operculum formation was not affected, however plasma membrane recession did not occur and no trilamellated structures formed (indicated by the red arrowhead; Fig. 1b and Extended Data Fig. 4b).

At the early vacuolated microspore stage (stage 10a), the wild-type plasma membrane in the aperture area continued to recede, and a lightly stained fibrillar-granular material layer formed in the gap between the aperture and the plasma membrane (Extended Data Fig. 4c). Mutant microspores at this stage exhibited the same changes but to a much lesser extent, with less recession of the plasma membrane from the aperture area and formation of a much thinner fibrillar-granular layer (Extended Data Fig. 4c). During the

late vacuolated microspore stage (stage 10b) in the wild type, the annulus became expanded with sporopollenin deposited on top and bottom surfaces of the trilamellated structures. Meanwhile, the developing vacuole forced the plasma membrane towards the wall and condensed the fibrillar-granular layer, which almost disappeared under the pressure of vacuolation in the mutant (Fig. 1b and Extended Data Fig. 4d).

At the binucleate pollen stage (stage 11), the fibrillar-granular layer in the wild-type pollen was further compressed under the operculum, beneath which developed a thick, moderately stained Zwischenkörper layer that was much thinner in the stage 11 mutant pollen (Extended Data Fig. 4e). At the mature pollen stage (stage 12), the complex aperture structure was completely formed in the wild-type pollen, with the bulging annulus surrounding the operculum, overlaying the fibrillar-granular and Zwischenkörper layers beneath the whole aperture (Fig. 1b and Extended Data Fig. 4f). Conversely, in the mutant pollen, the aperture lacked the annulus and the fibrillar-granular layer underneath the operculum, leading to a flattened, abnormal aperture (Fig. 1b and Extended Data Fig. 4f). These observations suggest that a defective aperture results in the abortion of most pollen and failure of pollen-tube germination in the rest, leading to complete male sterility.

OsDAF1 is a lectin receptor-like kinase. *osdaf1-1* was backcrossed with the 9522 parent for genetic and phenotypic analyses. All F_1 progeny displayed a normal phenotype, while F_2 progeny segregated 3:1 wild-type:mutant plants (260:76, $\chi^2 = 1.016$; $P > 0.05$), indicating that *osdaf1-1* male sterility is caused by a single recessive mutation. Moreover, pollination of the mutant pistil with wild-type pollen yielded entirely viable seeds, indicating that function of the female organ in *osdaf1-1* flowers is normal.

A map-based cloning approach was used to identify the gene responsible for the *osdaf1-1* phenotype, using 1,092 F_2 individuals. The mutated gene was mapped to chromosome 2 between two markers, Y3′ and YH42-5, defining a 4,138 kb region (Extended Data Fig. 5a). Sequencing revealed a 15-base pair (bp) deletion (bp 1527–1541) in the coding region of an annotated gene (LOC_Os02g26160; http://www.gramene.org/), causing a 5-amino-acid deletion in a conserved domain (Fig. 1c). Meanwhile, map-based cloning revealed that the *osdaf1-2* mutation was caused by a large insertion after bp 905 in the coding region of the same gene (Fig. 1c).

OsDAF1 encodes a 695-amino-acid protein belonging to the legume-lectin receptor-like kinase (L-Lec-RLK) family. These proteins comprise an N-terminal signal peptide, a putative carbohydrate-binding legume-lectin domain, a transmembrane region, and a serine/threonine protein kinase domain at the C-terminus (Fig. 1c). Quantitative real-time PCR revealed that *OsDAF1* was expressed in the rice anther, with the highest expression levels near the tetrad stage (stage 8; Extended Data Fig. 5b). We generated an independent mutation (*osdaf1-3*), using clustered regularly interspaced short palindromic repeats (CRISPR)–CRISPR-associated protein 9 (Cas9) to insert a single nucleotide in the lectin domain that created a premature stop codon after 175 amino acids (Fig. 1c); this mutant line exhibited an identical phenotype to *osdaf1-1* and *osdaf1-2* (Fig. 1a). Moreover, transformation of the wild-type *OsDAF1* gene under the control of its own promoter into the *osdaf1-1* mutant (*gOsDAF1 osdaf1-1*) restored the wild-type pollen phenotype and yielded viable seeds in all 26 T_0 transformants (Fig. 1a and Extended Data Fig. 1d,e), further confirming that LOC_Os02g26160 is *OsDAF1* and is required for pollen aperture formation and male fertility.

Lec-RLKs are widely distributed in higher plants and are often involved in stress response, innate immunity, symbiotic plant—fungal association, and plant development[26–29]. BLAST searches showed that OsDAF1-like proteins were highly conserved within grass species, which collectively harbour only one evident orthologue that shares approximately 75% identity with OsDAF1. Distant monocot or eudicot species contained a series of homologues sharing less than 45% identity with OsDAF1. These results suggest that *OsDAF1* and its orthologues could be the key factors required for the typical aperture pattern formation in grass species.

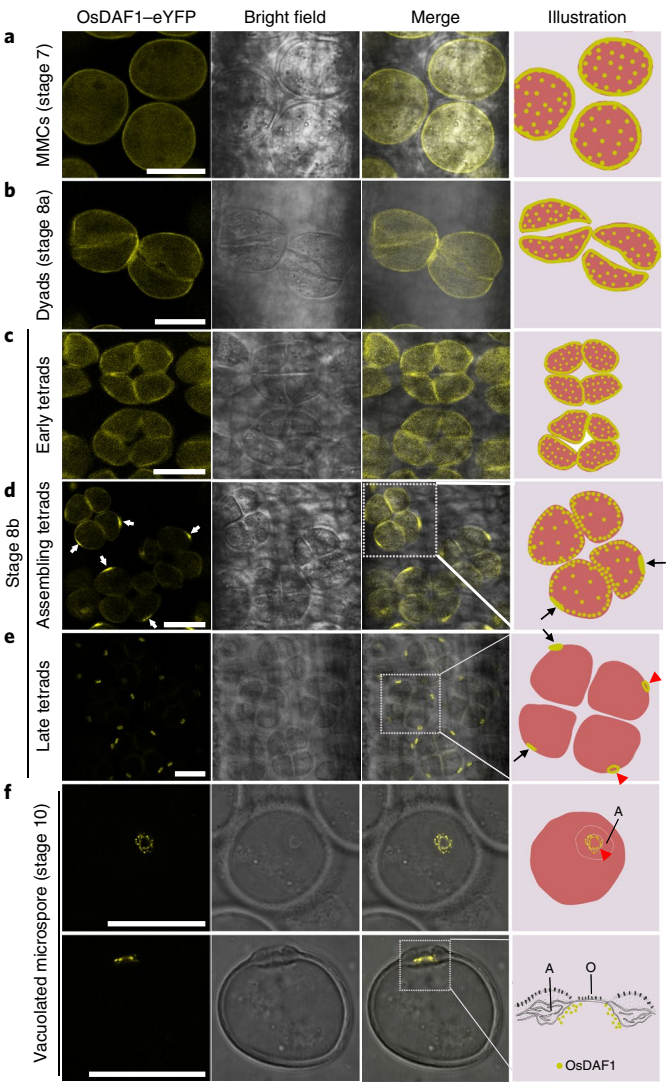

Fig. 2 | OsDAF1 assembles at future aperture sites. a–f, Confocal and bright-field imaging and illustrations of *OsDAF1:gOsDAF1-eYFP* plant anthers or microspores at MMC stage (stage 7) (**a**), dyad stage (stage 8a) (**b**), early tetrad stage (early stage 8b) (**c**), assembling tetrads stage (stage 8b) (**d**), late tetrad stage (stage 8b) (**e**) and vacuolated microspore stage (stage 10) (**f**). Arrows indicate the future aperture sites on the tetrad; arrowheads indicate the circular YFP signal at future aperture sites. A, annulus; O, operculum. These localizations were observed in three independent lines with similar results. Scale bars, 20 μm.

OsDAF1 assembles to future aperture sites at the tetrad stage. OsDAF1 possesses a putative transmembrane domain, and displayed uniform plasma membrane localization in both tobacco epidermal cells and rice protoplasts (Extended Data Fig. 6). To understand how OsDAF1 determines the polar distribution of the aperture structure, we analysed the localization of OsDAF1 protein in rice by expressing an OsDAF1–enhanced yellow fluorescent protein (eYFP) fusion protein. Using confocal microscopy, we found that in the meiotic stage (stage 7) rice anther, OsDAF1 was diffusely

distributed in the cytosol and plasma membrane of MMCs (Fig. 2a). After the first and second round of meiotic division, OsDAF1 remained diffusely distributed in dyads (stage 8a) and early tetrads (early stage 8b) (Fig. 2b,c). Within the same anther, slightly further developed tetrads started to show accumulated YFP signal at the corners (Fig. 2d). At late tetrad stage (late stage 8b), OsDAF1–eYFP signal clearly accumulated to the four corners of the tetrad, assembled into ring-like structures marking future aperture sites (Fig. 2e). When microspores were released from tetrads and preliminary aperture structures had formed (stage 9–10a), OsDAF1 remained in a distinctly ring-shaped distribution beneath the aperture in the plasma membrane between the annulus and operculum (Fig. 2f). The signals gradually disappeared at stage 10b (data not shown). Thus, the localization of OsDAF1 is consistent with its critical role in annulus formation, and suggests participation in formation of the fibrillar-granular layer during stage 9–10.

OsINP1 is required for aperture formation and OsDAF1 function. INP1 is involved in aperture formation in *Arabidopsis* and maize[20,21]. In rice, the INP1 homologue encodes a 232-amino-acid protein with no predicted signal peptide. To investigate whether OsINP1 is required for the pollen aperture formation in rice and its relationship with OsDAF1, we created *OsINP1* knockout mutations in wild-type and *osdaf1-1* plants. Two *osinp1* single mutants were obtained, each containing a single-nucleotide insertion at the same location that generated a premature stop codon in place of amino acid 165 (Fig. 3a). Similar to *atinp1*, both *osinp1* mutants developed seemingly normal anthers and pollen grains, but with a complete loss of aperture (Fig. 3b and Extended Data Fig. 7a), indicating that the roles of INP1 are conserved in *Arabidopsis* and rice. Anthers and pollen grains in a double *osinp1-1 osdaf1-1* mutant exhibited the same phenotype as *osinp1* single mutants. Notably, the double mutant rescued the phenotype of aborted pollen grains in the *osdaf1* single mutant (Fig. 3b and Extended Data Fig. 1f), indicating that OsINP1 is a prerequisite for OsDAF1 function, and the defective aperture in *osdaf1* mutants damages pollen stability during development. Similar to the *inp1* mutant in maize[21], the pollen of *osinp1* and *osinp1-1 osdaf1-1* was unable to germinate in vitro or in vivo (Fig. 3c and Extended Data Fig. 7b), suggesting that apertures are indispensable for rice pollen-tube germination and male fertility.

OsINP1 modifies the plasma membrane at aperture sites. Unlike OsDAF1, OsINP1 contains no predicted transmembrane domain and, accordingly, displayed ubiquitous distribution in tobacco epidermal cells (Extended Data Fig. 8). To test whether OsINP1 marks future aperture sites in rice—as does AtINP1 in *Arabidopsis*[20]—we introduced *OsINP1-eYFP* driven by the *OsINP1* promoter into wild-type rice plants. OsINP1 was uniformly distributed in the cytoplasm of MMCs during meiosis (stage 7), in dyads (stage 8a) and in the early tetrad stage (early stage 8b, Fig. 4a–c). In the late tetrad stage (late stage 8b), OsINP1 started to move to distal poles of the tetrad, concentrating into prominent spots (Fig. 4d). Finally, all tetrads displayed fluorescence specifically at the site that marks the future aperture, similar to OsDAF1 (Fig. 4e). After the release of the microspores (stage 9), we could see that similar to AtINP1–YFP in *Arabidopsis*, OsINP1–eYFP assumed a punctate distribution in a circular region corresponding to the area without sporopollenin in the future aperture, suggesting a conserved role of OsINP1 in preventing exine precursor deposition (Fig. 4f). When the preliminary aperture structure was formed at stage 10, OsINP1–eYFP fluorescence diminished into a few dots near the operculum (Fig. 4g) and degraded quickly as the microspore developed (data not shown), unlike OsDAF1–eYFP, which continued to emit a strong signal at this stage (Fig. 2f).

In *Arabidopsis*, AtINP1 was thought to be involved in keeping specific membrane domains close to the callose wall to prevent exine deposition at aperture sites[15,22]. To examine whether OsINP1 functions similarly in rice, we used a recently developed protocol[11] that enabled us to simultaneously visualize the YFP fluorescence, the plasma membrane and the callose wall. On wild-type tetrads, protruded plasma membrane could be observed at the future aperture sites (Extended Data Fig. 9a). Mutation of OsDAF1 did not affect this protrusion (Extended Data Fig. 9b), but on *osinp1* mutant tetrads, the plasma membrane smoothly covered the microspore surfaces (Extended Data Fig. 9c). Furthermore, combining plasma membrane staining with YFP fluorescence and callose-wall staining showed that OsINP1–eYFP coincided with the protrusion in wild-type plants and stretched into the callose wall (Extended Data Fig. 9d). These findings demonstrate that, similar to AtINP1

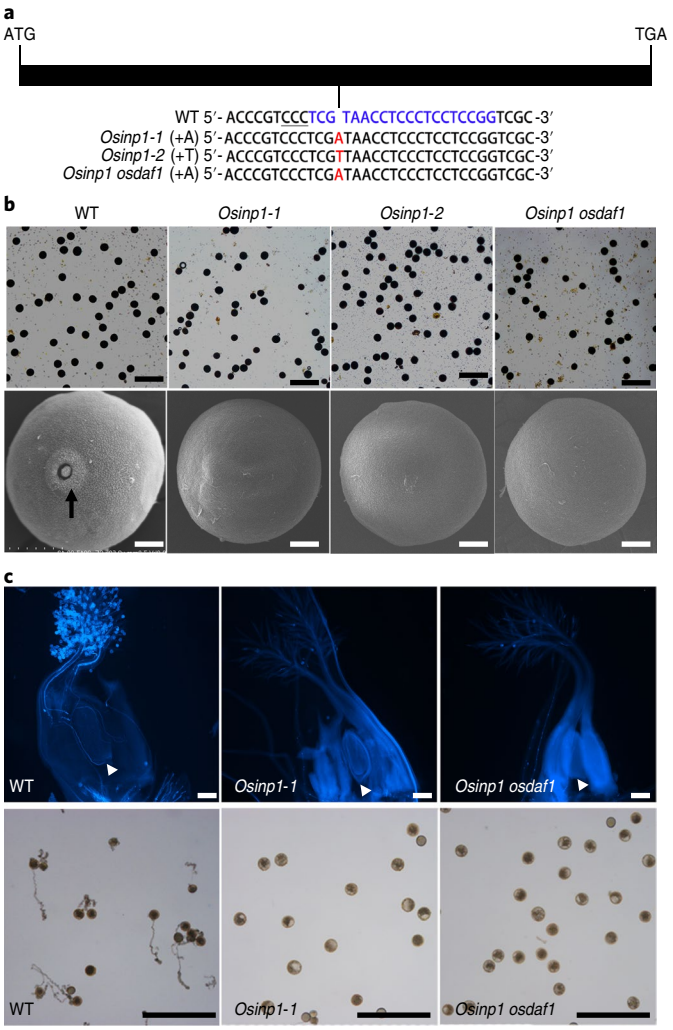

Fig. 3 | *osinp1* is epistatic to *osdaf1*. a, CRISPR–Cas9-mediated targeted mutagenesis of *OsINP1*. The *OsINP1* gene, indicating the CRISPR–Cas9 target site, is represented by a thick black line. An alignment of wild-type (WT), *osinp1-1*, *osinp1-2* and *osinp1 osdaf1* sequences shows the 1-bp insertion of A or T (red) at the target site. The 20-bp CRISPR–Cas9 target sequence adjacent to the underlined protospacer adjacent motifs is indicated in blue. **b**, Comparison of mature wild-type, *osinp1-1* and *osinp1 osdaf1* pollen grains by I_2-KI staining (top) and SEM (bottom). Aborted pollen grains do not stain dark blue with iodine. The arrow indicates the aperture. **c**, In vivo (top) and in vitro (bottom) pollen-germination assays of wild type, *osinp1-1* and *osinp1 osdaf1*. Arrowheads indicate the ovules. Phenotypes in **b**,**c** were observed at least three times independently with similar results. Scale bars: 100 μm (**b**, top), 5 μm (**b**, bottom) and 200 μm (**c**).

in *Arabidopsis*, OsINP1 participates in the modification of plasma membrane at future aperture sites, possibly by creating close contact between the plasma membrane and callose wall to prevent primexine formation and sporopollenin deposition.

OsDAF1 interacts with OsINP1. On the basis of the related phenotypes and similar protein locations of OsDAF1 and OsINP1 in rice, we speculated that these two proteins might interact to promote rice aperture formation. We employed different approaches to test in vitro and in vivo interactions between OsDAF1 and OsINP1. Yeast two-hybrid analysis using the N-terminal extracellular (OsDAF1(N)) and C-terminal intracellular (OsDAF1(C)) domains of OsDAF1 with the full-length OsINP1 protein (Fig. 5a) revealed that only OsDAF1(C) was able to interact with OsINP1 (Fig. 5b). Moreover, the C-terminus of the *osdaf1-1* mutated protein (OsDAF1(Δ5-C)) was unable to interact with OsINP1 (Fig. 5b), whereas its localization or stability in tobacco was not affected (Extended Data Fig. 10), suggesting that these deleted five amino acids are critical for mediating DAF1—INP1 interactions in wild-type plants. These amino acids may also have a role in OsDAF1 kinase activity. Interaction between OsDAF1(C) and OsINP1 was further confirmed by bimolecular fluorescence complementation (BIFC) experiments in living tobacco cells (Fig. 5c), split-luciferase assays using a transient expression system in tobacco leaves (Fig. 5d), and co-immunoprecipitation analysis using tobacco leaf extracts (Fig. 5e).

The C-terminus of OsDAF1 directs polar distribution. To examine the in vivo location of each protein in the absence of the other protein, we introduced *OsINP1-eYFP* into *osdaf1-1* and *OsDAF1-eYFP* into *osinp1-1* mutants. Consistent with the observation that the operculum and circular region without sporopollenin were present in *osdaf1* (Fig. 1a,b), the *OsDAF1* mutation did not affect the polar location of OsINP1–YFP (Fig. 6a), indicating that OsINP1 localizes and functions normally in the absence of OsDAF1. However, the polar distribution of OsDAF1–eYFP was clearly disrupted in the absence of functional OsINP1. OsDAF1 failed to assemble at the future aperture sites, instead spreading evenly across the plasma membrane throughout the tetrad cells (Fig. 6b). Moreover, OsDAF1 did not promote annulus formation on any area of *osinp1* mutant pollen (Fig. 3b). This result strongly indicates that OsDAF1 is recruited to the correct subcellular location via interaction with OsINP1, and functions only at the future aperture sites. To further investigate the functions of OsDAF1 protein domains, we generated truncated versions of OsDAF1 fused with eYFP driven by the native promoter (Fig. 6c). When the C-terminal kinase domain of OsDAF1 was lost, YFP signal was diffused throughout the plasma membrane during the tetrad stage (Fig. 6d), supporting findings from mutant phenotyping (Fig. 1) and protein interaction (Fig. 5) experiments that the C-terminal kinase domain is essential for the recruitment and localization of OsDAF1. When the N-terminal signal peptide and lectin domain were missing, the fluorescence signal completely disappeared (Fig. 6e). In addition, full-length OsDAF1–eYFP proteins without the signal peptide driven by 35S promoter in tobacco also displayed no YFP signal or detectable protein expression, suggesting that the signal peptide is essential for OsDAF1 protein stability (Extended Data Fig. 10). A truncated protein missing only the lectin domain successfully assembled to the future aperture sites (Fig. 6f).

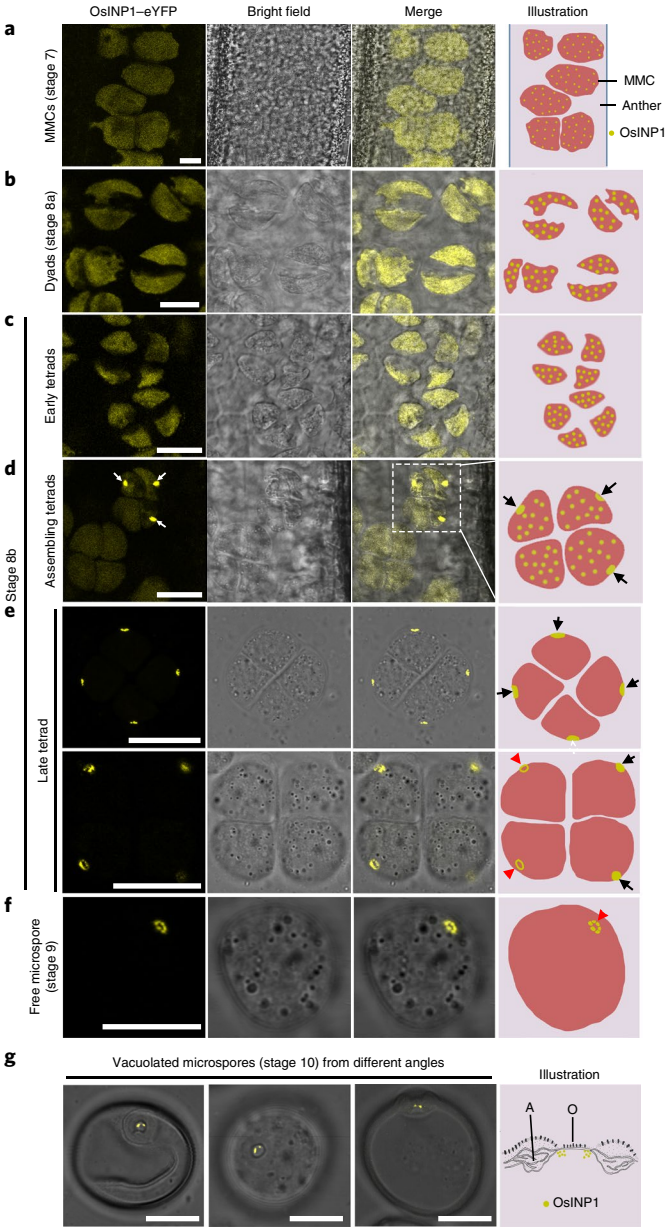

Fig. 4 | OsINP1 localizes to future aperture sites. a–g, Confocal images and illustrations of *OsINP1:gOsINP1-eYFP* plant anthers or microspores at MMC stage (stage 7) (**a**), dyad stage (stage 8a) (**b**), early tetrad stage (stage 8b) (**c**), assembling tetrads stage (stage 8b) (**d**), late tetrad stage (stage 8b) (**e**), free microspore stage (stage 9) (**f**) and vacuolated microspores (stage 10) (**g**) from different angles. Arrows indicate the future aperture sites on the tetrad; arrowheads indicate the circular YFP signal at future aperture sites. A, annulus; O, operculum. These localizations were observed in three independent lines with similar results. Scale bars: 20 μm (**a**–**e**) and 10 μm (**f**,**g**).

Discussion

The morphology of the pollen aperture is highly diversified in nature, suggesting the active reprogramming of the molecular machineries driving pollen aperture formation during evolution. However, the underlying mechanisms leading to the different aperture patterns have remained unknown. *Arabidopsis* and rice pollen possess highly typical forms of eudicot and grass apertures, respectively, providing excellent models to solve this puzzle. *Arabidopsis* pollen grains contain three equidistant and equatorially arrayed furrow-like apertures where no sporopollenin is deposited, and which display no obvious additional structures. *Arabidopsis* INP1 has been reported to function as a late-acting factor in pollen aperture formation[20,22]. AtINP1 is recruited to future aperture positions after cytokinesis at the tetrad stage, preventing the formation of primexine and the subsequent sporopollenin deposition by maintaining close contact between the plasma membrane and the callose wall. By contrast,

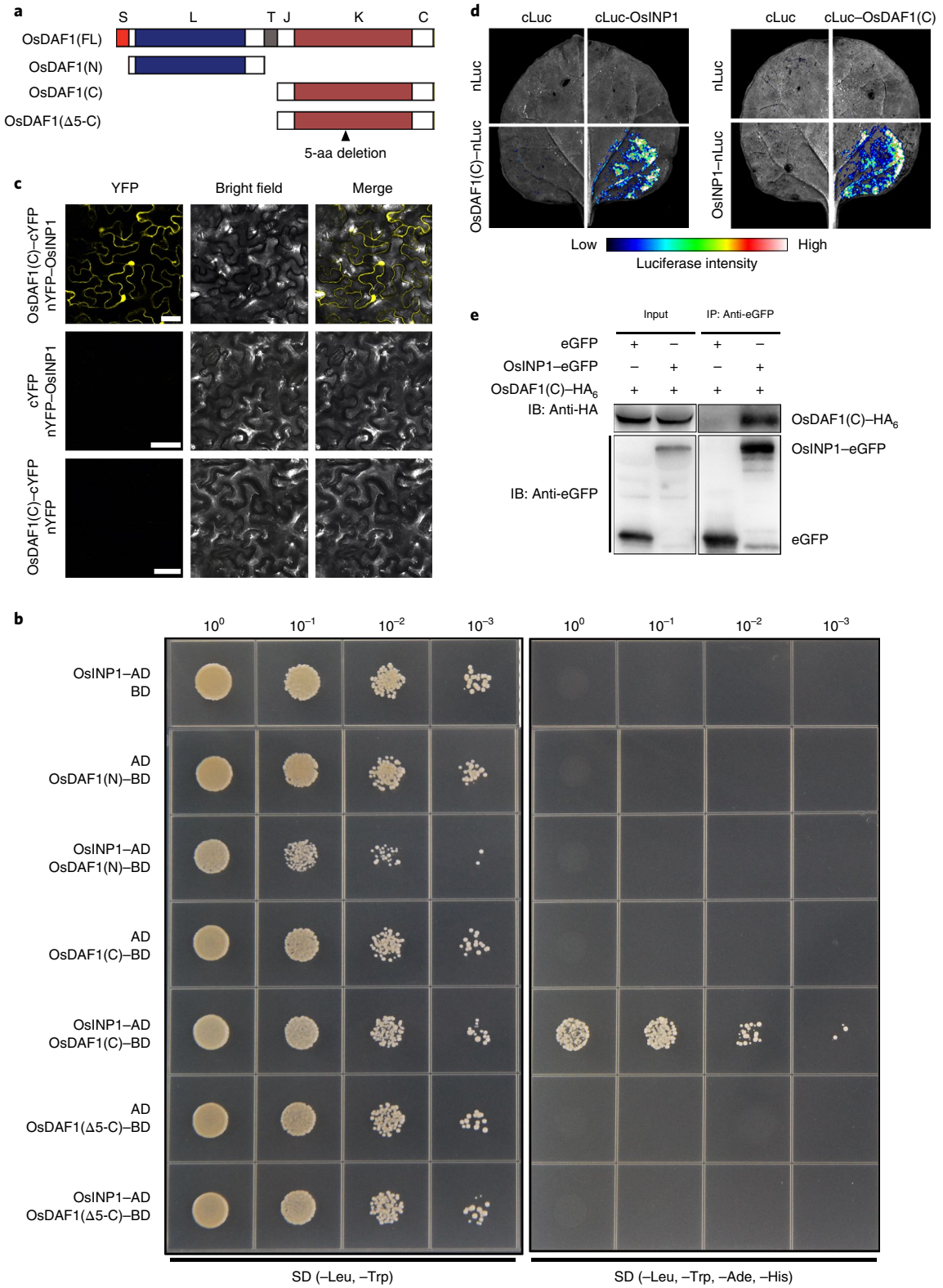

Fig. 5 | The C terminus of OsDAF1 interacts with OsINP1. a, Schematic diagrams of truncated or mutated OsDAF1 proteins. The full-length (FL) OsDAF1 protein including the signal peptide (S; amino acids 1–23), lectin domain (L; amino acids 35–286), transmembrane domain (T; amino acids 332–354), juxtamembrane region (J; amino acids 355–388), kinase domain (K; amino acids 389–654) and C-terminal region (C; amino acids 655–695) is presented at the top. OsDAF1(N) contains only the lectin domain; OsDAF1(C) contains the J, K and C regions; OsDAF1(Δ5-C) contains the J, K and C regions with the same five-amino-acid deletion as the *osdaf1-1* mutant (see Fig. 1c). aa, amino acid. **b**, Yeast two-hybrid assay of interaction between OsINP1 and truncated or mutated OsDAF1. AD, activating domain; BD, DNA-binding domain; SD, synthetic defined medium. **c**, BIFC assay between OsINP1 and OsDAF1(C) in *Nicotiana benthamiana*. nYFP, N-terminal yellow fluorescent protein; cYFP, C-terminal yellow fluorescent protein. Scale bars, 50 μm. **d**, Split-luciferase assays between OsDAF1(C) and OsINP1 with controls. cLuc, C-terminal luciferase; nLuc, N-terminal luciferase. **e**, Co-immunoprecipitation assay with co-expression of OsINP1–eGFP and haemagglutinin (HA)-tagged OsDAF1(C) (OsDAF1(C)–HA_6) in tobacco leaves. IP, immunoprecipitation; IB, immunoblot. All experiments were repeated three times with similar results.

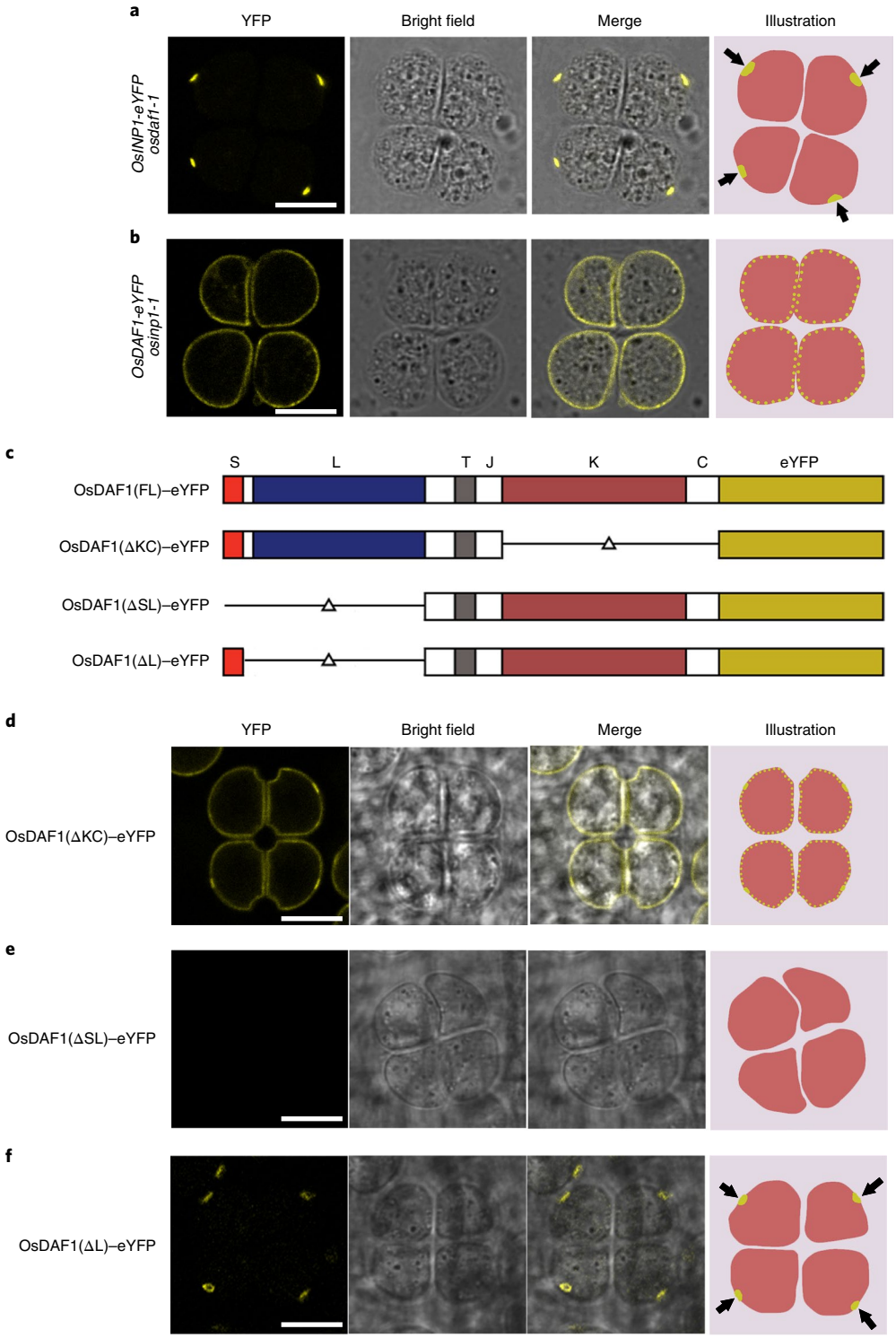

Fig. 6 | Interaction with OsINP1 is essential for OsDAF1 localization. a,**b**, Confocal and bright-field images and illustrations of OsINP1 localization in tetrads of *osdaf1-1* mutant (**a**) and OsDAF1 localization in tetrads of *osinp1-1* mutant (**b**). **c**, Schematic diagrams of full-length and truncated OsDAF1 proteins fused with eYFP. **d**–**f**, Localization and illustration of truncated OsDAF1 proteins in wild-type tetrads. These localizations were observed at least three times independently with similar results. Arrows indicate the future aperture sites on the tetrad. Scale bars, 10 μm.

rice pollen has a complex, distally positioned aperture structure comprising an annulus and an operculum. In this study, we reveal that rice INP1 interacts with OsDAF1, a legume-lectin receptor-like kinase, to regulate formation of this grass-specific aperture pattern.

Like AtINP1, OsINP1 is anchored to future aperture sites soon after tetrad formation, where it modifies the plasma membrane to permit formation of membrane protrusions. The protruding membrane remains in the vicinity of the callose wall, thus preventing primexine formation and sporopollenin deposition (Fig. 4 and Extended Data Fig. 9). These observations suggest that OsINP1 has similar biochemical functions to AtINP1, and has a conserved role in aperture formation by preventing sporopollenin deposition

at aperture sites. Our study also reveals additional roles of OsINP1 in rice aperture formation, where it also directs annulus formation by interacting with OsDAF1 (Figs. 1, 5, 6). Furthermore, OsINP1 seems to be involved in operculum protrusion—probably due to the presence of the fibrillar-granular and Zwischenkörper layers in wild-type pollen (Fig. 1b and Extended Data Fig. 4f)—that is completely absent in *osinp1* mutants (Fig. 3b).

OsDAF1 is distributed both in the cytoplasm and on the plasma membrane of male meiocytes during meiosis. At early tetrad stage, OsDAF1 becomes evenly distributed in the plasma membrane of microspores; this distribution is not dependent on OsINP1 (Fig. 6). However, polar accumulation of OsDAF1 at four distal points of the tetrad is determined by the interaction with OsINP1 via its intracellular C-terminal domain (Figs. 5 and 6). Conversely, the polarization of OsINP1 does not depend on OsDAF1 function (Fig. 6). These results suggest that the arrival of OsINP1 at future aperture sites is required for further specification of the future annulus and/or operculum formation.

Polarized protein localization is one of the most prevalent strategies employed to control asymmetric cell division in animals and plants[30]. One prominent example is the stomatal asymmetric division driven by the polarization of BREAKING OF ASYMMETRY IN THE STOMATAL LINEAGE (BASL). Recent reports suggest that BASL acts as a scaffold protein to polarize the MAPKK kinase YODA and MAPK 3/6/K to the cortical polarity site[30,31]. OsINP1 may also serve as a scaffold protein to direct the localization of OsDAF1. Discovery of the role of OsDAF1 in rice pollen aperture formation and its relationship with OsINP1 provides important insights into the mechanism of cell-surface patterning and polarity control in grass pollen. By contrast, although AtD6PKL3 and AtINP1 influence each other's polarized localization, they do not directly interact[23]. The difference may reflect different strategies plant cells use to define distinct membrane domains. The association of AtD6PKL3 with the plasma membrane domain at future aperture sites depends on the presence of its lipid-binding lysine/arginine-rich motif, probably through its binding to the phospholipids enriched at these sites. Thus, AtD6PKL3 might contribute to the recruitment of AtINP1 by modifying the plasma membrane in these areas, but not via direct interaction with AtINP1.

Legume Lec-RLK family proteins are usually involved in plant–microbe interactions, and in a few cases, are related to plant development[29,32]. OsDAF1 in rice, however, is essential for pollen development and exhibits distinct polar distribution, which, to our knowledge, had not been previously observed in Lec-RLK proteins. OsDAF1 contains the canonical Lec-RLK N-terminal extracellular ligand-binding domain and C-terminal intracellular kinase domain; five amino acids in the kinase domain are critical for mediating the interaction with OsINP1 and therefore correct protein function. However, the downstream kinase-activated signalling pathway remains unclear, and further research focusing on the upstream and downstream pathways involving OsDAF1 will facilitate understanding of both pollen aperture formation and Lec-RLKs family functions. Previous studies in *Arabidopsis* revealed that *INP1* mutation leads to loss of all pollen apertures, but normal pollen-tube germination and fertility is retained, indicating that a pollen aperture is not essential for *Arabidopsis* reproduction[20,21]. By contrast, apertures are indispensable for pollen germination and male fertility in the commercially important cereal species[21]. In this study, we have shown that the *osdaf1* mutation, which causes complete disappearance of the annulus, results in abortion of most pollen grains. Interestingly, mutation of *OsINP1* in the *osdaf1* background prevented abortion of pollen grains but did not restore male fertility. In addition, we found that the proportion of aborted pollen grains was higher with higher environmental temperature over five different years at the same growing location (Supplementary Fig. 1). These observations suggest that the aperture is not essential for the normal development of rice pollen, but that a defective aperture increases pollen fragility, especially when grown at higher temperatures. Thus, the presence of a correctly formed pollen aperture is critical for rice fertility.

How the underdeveloped aperture suppresses rice pollen grain viability has not been fully understood. The aperture is required for both pollen-tube germination and for water uptake and exit, as microspores undergo several rounds of shrinkage and expansion during maturation. An integrated aperture structure might be required to seal the inside of the pollen grains to accommodate volume change and prevent loss of cytoplasmic components. In *Arabidopsis*, mutant pollen grains with larger numbers of apertures became more vulnerable to volume change during rehydration[16,17], supporting the idea that a normal aperture pattern is essential for pollen viability and performance. OsDAF1 may also contribute to other aspects of pollen development that are important for pollen maturation in addition to aperture formation. Recently, Peng et al. reported another mutant allele of *osdaf1*, *s13283*, which exhibited similar pollen aperture defects[33]. They showed that *s13283* was also defective in pollen wall formation, including pollen exine and intine[33]. Although *osdaf1* mutants displayed no obvious morphological change in the pollen exine (Supplementary Fig. 2a), the intine became thinner or absent in *osdaf1* mature pollen (Supplementary Fig. 2b). Whether the defective intine is a direct or indirect consequence of *OsDAF1* disruption remains to be determined. Understanding the mechanisms of aperture formation would be beneficial for translational agricultural research, providing tools to safeguard cereal productivity and food security.

Methods

Plant materials, growth conditions and cloning of *OsDAF1*. Rice (*O. sativa*) plants were grown in the paddy field at Shanghai Jiao Tong University during the natural growing season. The F_2 mapping population was generated from a cross between the *osdaf1* mutant (*japonica*) and Guangluai 4 (wild type, *indica*). Male sterile plants in the F_2 progeny were selected for gene mapping. To fine-map the *OsDAF1* locus, bulked segregant analysis[34] was used, and insertion-deletion (indel) molecular markers were designed on the basis of the sequence differences between *japonica* and *indica* described in the NCBI database. The *OsDAF1* locus was first mapped between two indel molecular markers: Os205 and Os206. Then, 1092 F2 segregants from the mapping cross were generated, and eight indel markers were used. *OsDAF1* was eventually located between Y3′ and YH42-5 within a 4,138-kb region (Extended Data Fig. 5a). All primers used in the mapping are listed in Supplementary Table 1.

Characterisation of the mutant phenotype. Morphological images of whole rice plants were captured with a Nikon E995 digital camera. Images of flowers such as fresh spikelets, opened flowers and dehiscent anthers were photographed with a Leica M205A microscope. For pollen viability analysis, anthers were immersed into Lugol's iodine (I_2-KI) solution and crushed with tweezers, and released pollen grains were photographed with a Nikon Eclipse 80i microscope. Transverse section analysis of developing anthers was carried out by the Technovit Embedding Kits (Heraeus Kulzer) as described previously[35]. For scanning electron microscopic (SEM) observations, flowers were fixed in formaldehyde/acetic acid/ethanol solution for 2 h and dehydrated with a 40, 50, 60, 70, 80, 90, 95 and 100% ethanol series. The samples were dried using a Leica EM CPD300 automated critical dryer, and the dried samples were coated with gold using a cool sputter coater (Leica EM SCD005). Anther and pollen grain surfaces were photographed under a SEM (Hitachi S3400N). TEM analysis was performed as described[35]. Ultrathin transverse sections were double stained with 2% (w/v) uranyl acetate and 2.6% (w/v) lead citrate aqueous solution, and examined with a Tecnai G2 spirit Biotwin TEM.

In vitro pollen-germination assays. In vitro pollen germination was performed as described[36]. In brief, rice pollen grains were collected by gently shaking panicles in the paddy field into a liquid germination medium (20% (w/v) sucrose, 10% (w/v) polyethylene glycol 4000, 3 mM $Ca(NO_3)_2{\cdot}4H_2O$, 40 mg l^{-1} H_3BO_3 and 3 mg l^{-1} vitamin B1) and cultured for 10 min at room temperature (30 °C) under moist conditions to generate synchronously germinated rice pollen grains.

Aniline blue staining of pollen tubes in vivo. In vivo pollen-tube growth was performed as described previously[36]. In brief, at 6 h after pollination, rice pistils were cut and fixed in Carnoy's solution overnight. The pistils were then washed 5 times with water, softened by incubating in 1 M NaOH at 55 °C for 30 min and stained in 0.1% (w/v) aniline blue (in 0.1 M K_2HPO_4, pH 8.5) at room temperature

for 4–16 h in the dark. Fluorescent images were observed with an Eclipse Ni-E microscope (Nikon) under UV light.

Transgenic constructs. For functional complementation, a 7,233 bp genomic sequence of *OsDAF1*, which contains the entire *OsDAF1* coding region (2,088 bp), a 2,890 bp upstream sequence and a 2,255 bp downstream sequence, was amplified from wild-type rice genome DNA. The genomic fragment was cloned into the binary vector pCAMBIA1301 (CAMBIA) and transformed into *osdaf1-1* calli to create the rescued *gOsDAF1 osdaf1-1* line. To create the *OsDAF1*$_{pro}$*:OsDAF1-eYFP-3′UTR* construct for protein localization in rice, *eYFP* gene was inserted between the *OsDAF1* coding sequence (without stop codon) and the 2,255 bp downstream sequence, and subsequently transformed into *osdaf1-1* calli.

CRISPR–Cas9-knockout mutants of *OsINP1* in wild-type or *osdaf1-1* background were obtained using the methods as previously described[37]. To create the *OsINP1*$_{pro}$*:OsINP1-eYFP* construct for protein localization in rice, 2,259 bp upstream sequence and 696 bp coding sequence (without stop codon) were amplified from wild-type rice genomic DNA. The genomic fragment was cloned into the modified binary vector pCAMBIA1301-eYFP. The *OsINP1*$_{pro}$*:OsINP1-eYFP* construct was subsequently transformed into wild-type rice calli.

Constructs for localization of truncated OsDAF1 proteins in rice were obtained based on the *OsDAF1*$_{pro}$*:OsDAF1-eYFP-3′UTR* construct. We first amplified the *eYFP-3'UTR* fragment and cloned it into the binary vector pCAMBIA1301 to create *1301-eYFP-3′UTR* as backbone for further construction. For the *OsDAF1*$_{pro}$*:OsDAF1ΔKC-eYFP-3′UTR* construct, we amplified the *OsDAF1*$_{pro}$*:OsDAF1ΔKC* fragments (OsDAF1 CDS without kinase domain and C-terminal region) and inserted them into *1301-eYFP-3′UTR* upstream of *eYFP*. For the *OsDAF1*$_{pro}$*:OsDAF1ΔSL-eYFP-3′UTR* construct, we first amplified the *OsDAF1*$_{pro}$ fragment and placed it into *1301-eYFP-3′UTR* upstream of *eYFP*; we then amplified the *OsDAF1ΔSL* fragment (OsDAF1 coding sequence without signal peptide and lectin domain, plus start codon and minus stop codon) and cloned it between *OsDAF1*$_{pro}$ and *eYFP*. For the *OsDAF1*$_{pro}$*:OsDAF1ΔL-eYFP-3′UTR* construct, we first amplified the *OsDAF1*$_{pro}$*:sp* fragment (*OsDAF1* promoter region and signal peptide) and placed it into *1301-eYFP-3′UTR* upstream of *eYFP*; we then amplified the same *OsDAF1ΔSL* fragment without adding the additional start codon, and cloned it between *OsDAF1*$_{pro}$*:sp* and *eYFP*. These constructs were subsequently transformed into wild-type rice calli. All primers used for constructs are listed in Supplementary Table 1.

Expression analysis. Total RNA was extracted from wild-type rice anther at different developmental stages using Trizol Reagent (Invitrogen). Development stages of wild-type and mutant anthers were as defined in ref. [8]. One microgram of RNA per sample was used to synthesize cDNA using the Primescript1 RT reagent kit with gDNA eraser (Takara). Quantitative PCR with reverse transcription was performed on the Bio-Rad C1000 thermal cycler using SYBR Premix Ex Taq GC (Takara). The Rice *ACTIN* gene was used as the internal control. Data analysis was performed as previously described[38]. Three replicates were performed for each experiment. Primers used for PCR amplification are listed in Supplementary Table 1.

Subcellular localization assay. The coding regions of OsDAF1 and OsINP1 were amplified and cloned into pHB-35S$_{pro}$-eYFP and pHB-35S$_{pro}$-eGFP, respectively. The recombinant and empty vectors were transformed into *A. tumefaciens* GV3101. After centrifugation, the bacteria were collected and resuspended in infection solution (10 mM MES, 10 mM $MgCl_2$ and 200 μM acetosyringone) for infiltration (at $A_{600\,nm} = 0.6$). The prepared suspensions were infiltrated into *N. benthamiana* leaves and grown in the dark for 2 d. Fluorescent signals of eGFP or eYFP were monitored using a Leica SP8 confocal microscope (Leica TCS SP8 X, excitation 514 nm, emission 522–555 nm for eYFP; excitation 488 nm, emission 500–550 nm for eGFP).

Confocal microscopy for rice microsporocytes and microspores. For imaging microsporocytes before tetrad stage, stage 7–8 anthers were dissected from flowers and placed into 20% glycerol for microscopy. For free microspores after meiosis, stage 9–10 anthers were dissected from flowers and placed into 20% glycerol, with gentle pressure applied using a coverslip to release microspores for imaging. Fluorescent signals of eYFP were monitored using a Leica SP8 confocal microscope (Leica TCS SP8 X, excitation 514 nm; emission 522–555 nm).

Confocal microscopy of stained tetrads was performed as described previously, with modifications[22]. In brief, stage 8 rice anthers were dissected from flowers and placed into 20% glycerol supplemented with 0.02% calcofluor white and 5 mg ml^{-1} membrane stain CellMask Deep Red (Molecular Probes). Anthers were crushed with tweezers to release stained tetrads for imaging (Leica SP8 confocal microscope with a ×100 oil-immersion objective; excitation 514 nm, emission 522–555 nm for eYFP; excitation 405 nm, emission 424–475 nm for calcofluor white; excitation 640 nm, emission 663–738 nm for CellMask Deep Red dye).

Yeast two-hybrid assay. The coding sequences of *OsINP1* and truncated or mutated *OsDAF1* were amplified and cloned into pGBKT7 or pGADT7 (Clontech) and then transformed into the yeast stain AH109. The yeast two-hybrid assays were performed according to the manufacturer's instructions (Clontech).

BIFC assay. The coding region of *OsINP1* and C-terminal *OsDAF1* were amplified and cloned into pXY106-nYFP and pXY104-cYFP plasmids, respectively. The recombinant vectors were co-transformed into *Agrobacterium tumefaciens* GV3101. After centrifugation, the bacteria were collected and resuspended in infection solution (10 mM MES, 10 mM $MgCl_2$ and 200 μM acetosyringone) for infiltration (at $A_{600} = 0.6$). The prepared suspensions were infiltrated into *N. benthamiana* leaves and grown in the dark for 2 d. Fluorescent eYFP signals were monitored using a Leica SP8 confocal microscope (Leica TCS SP8 X, excitation 514 nm; emission 522–555 nm).

Split-luciferase assay. The coding regions of *OsINP1* and C-terminal *OsDAF1* were amplified and each cloned into pCAMBIA 1300-cLuc and pCAMBIA 1300-nLuc plasmids. The recombinant vectors were co-transformed into *A. tumefaciens* GV3101 and infiltrated into *N. benthamiana* leaves as described above, and grown in the dark for 40 h. The leaves were then sprayed with 5 mM luciferin and kept in the dark for 10 min to quench the fluorescence. A cooling CCD imaging apparatus (Tanon-5200) was used for image capture.

Co-immunoprecipitation assays. The coding region of C-terminal OsDAF1 was amplified and cloned into pGreen-35S$_{pro}$-6HA; the coding region of OsINP1 was amplified and cloned into pHB-35S$_{pro}$-eGFP. The recombinant vectors were co-transformed into *A. tumefaciens* GV3101 and infiltrated into *N. benthamiana* leaves as described above, and grown in the dark for 3 d before collection. The subsequent procedures were conducted as previously described[39]. Total protein was extracted from infiltrated tobacco leaves with protein extraction buffer (50 mM Tris-HCl (pH 7.5), 100 mM NaCl, 1 mM EDTA, 10 mM NaF, 5 mM Na_3VO_4, 0.25% Triton X-100, 0.25% NP-40, 1 mM PMSF and 1× protease inhibitor cocktail) and then incubated with 20 μl anti-GFP agarose beads (Chromotek, gta-20) for 2 h at 4 °C. The beads were washed five times with wash buffer (50 mM Tris-HCl (pH 7.5), 100 mM NaCl, 1 mM EDTA, 1 mM PMSF and 1× protease inhibitor cocktail) and the precipitated proteins were eluted with 2× SDS loading buffer at 95 °C for 3 min. The samples were analysed by immunoblotting using the indicated antibodies. Commercial antibodies used were: GFP (G1544, Sigma, 1:5,000 dilution), haemagglutinin (M20003, Abmart, 1:2,000 dilution), goat anti-mouse IgG–horseradish peroxidase (HRP) conjugate (M21001, Abmart, 1:5,000 dilution), goat anti-rabbit IgG–HRP conjugate (M21002, Abmart, 1:5,000 dilution).

Truncated OsDAF1 expression level in tobacco. The coding region of full-length or the corresponding truncated version OsDAF1 was amplified and cloned into pHB-35S$_{pro}$-GFP or pHB-35S$_{pro}$-YFP. The recombinant vectors were transformed into *A. tumefaciens* GV3101 and infiltrated into *N. benthamiana* leaves as described above, and grown in the dark for 3 d before harvesting. Total protein was extracted from infiltrated tobacco leaves as described above, and analysed by immunoblotting using the indicated antibodies. Commercial antibodies used were: GFP (G1544, Sigma, 1:5,000 dilution), actin (M20009, Abmart, 1:2,000 dilution), goat anti-mouse IgG–HRP conjugate (M21001, Abmart, 1:5,000 dilution), goat anti-rabbit IgG–HRP conjugate (M21002, Abmart, 1:5000 dilution).

Reporting Summary. Further information on research design is available in the Nature Research Reporting Summary linked to this article.

Data availability

Source Data for Fig. 5 and Extended Data Fig. 10 are provided with the paper. Sequence data from this article can be found in the Rice Genome Annotation Project (http://rice.plantbiology.msu.edu) under accession numbers LOC_Os02g26160 (OsDAF1) and LOC_Os02g44250 (OsINP1). The data that support the findings of this study are available from the corresponding author upon reasonable request.

Received: 14 October 2019; Accepted: 28 February 2020;
Published online: 13 April 2020

References

1. Shi, J., Cui, M., Yang, L., Kim, Y. J. & Zhang, D. Genetic and biochemical mechanisms of pollen wall development. *Trends Plant Sci.* **20**, 741–753 (2015).
2. Ariizumi, T. & Toriyama, K. Genetic regulation of sporopollenin synthesis and pollen exine development. *Annu. Rev. Plant Biol.* **62**, 437–460 (2011).
3. Li, F.-S., Phyo, P., Jacobowitz, J., Hong, M. & Weng, J.-K. The molecular structure of plant sporopollenin. *Nat. Plants* **5**, 41–46 (2019).
4. Quilichini, T. D., Grienenberger, E. & Douglas, C. J. The biosynthesis, composition and assembly of the outer pollen wall: a tough case to crack. *Phytochemistry* **113**, 170–182 (2015).
5. Furness, C. A. & Rudall, P. J. Pollen aperture evolution—a crucial factor for eudicot success? *Trends Plant Sci.* **9**, 154–158 (2004).
6. Edlund, A. F. Pollen and stigma structure and function: the role of diversity in pollination. *Plant Cell* **16**, S84–S97 (2004).
7. McCormick, S. Control of male gametophyte development. *Plant Cell* **16**, 142–154 (2004).

8. Zhang, D., Luo, X. & Zhu, L. Cytological analysis and genetic control of rice anther development. *J. Genet. Genomics* **38**, 379–390 (2011).
9. Ma, H. Molecular genetic analyses of microsporogenesis and microgametogenesis in flowering plants. *Annu. Rev. Plant Biol.* **56**, 393–434 (2005).
10. Wang, R. & Dobritsa, A. Exine and aperture patterns on the pollen surface: their formation and roles in plant reproduction. *Annu. Plant Rev.* **1**, 1–40 (2018).
11. Dobritsa, A. A. & Reeder, S. H. Formation of pollen apertures in *Arabidopsis* requires an interplay between male meiosis, development of INP1-decorated plasma membrane domains, and the callose wall. *Plant Signal. Behav.* **12**, e1393136 (2017).
12. Reeder, S. H., Lee, B. H., Fox, R. & Dobritsa, A. A. A ploidy-sensitive mechanism regulates aperture formation on the *Arabidopsis* pollen surface and guides localization of the aperture factor INP1. *PLoS Genet.* **12**, e1006060 (2016).
13. Albert, B., Ressayre, A. & Nadot, S. Correlation between pollen aperture pattern and callose deposition in late tetrad stage in three species producing atypical pollen grains. *Am. J. Bot.* **98**, 189–196 (2011).
14. Nadot, S., Forchioni, A., Penet, L., Sannier, J. & Ressayre, A. Links between early pollen development and aperture pattern in monocots. *Protoplasma* **228**, 55–64 (2006).
15. Toghranegar, Z., Nadot, S. & Albert, B. Variation of microsporogenesis in monocots producing monosulcate pollen grains. *Ann. Bot.* **112**, 135–139 (2013).
16. Albert, B. et al. Effect of aperture number on pollen germination, survival and reproductive success in *Arabidopsis thaliana*. *Ann. Bot.* **121**, 733–740 (2018).
17. Prieu, C. et al. Aperture number influences pollen survival in *Arabidopsis* mutants. *Am. J. Bot.* **103**, 452–459 (2016).
18. Köhler, E. & Lange, E. A contribution to distinguishing cereal from wild grass pollen grains by LM and SEM. *Grana* **18**, 133–140 (1979).
19. El-Ghazaly, G. & Jensen, W. A. Studies of the development of wheat (*Triticum aestivum*) pollen. *Grana* **25**, 1–29 (1986).
20. Dobritsa, A. A. & Coerper, D. The novel plant protein INAPERTURATE POLLEN1 marks distinct cellular domains and controls formation of apertures in the *Arabidopsis* pollen exine. *Plant Cell* **24**, 4452–4464 (2012).
21. Li, P. et al. INP1 involvement in pollen aperture formation is evolutionarily conserved and may require species-specific partners. *J. Exp. Bot.* **69**, 983–996 (2018).
22. Dobritsa, A. A., Kirkpatrick, A. B., Reeder, S. H., Li, P. & Owen, H. A. Pollen aperture factor INP1 acts late in aperture formation by excluding specific membrane domains from exine deposition. *Plant Physiol.* **176**, 326–339 (2018).
23. Lee, B. H. et al. *Arabidopsis* protein kinase D6PKL3 is involved in the formation of distinct plasma membrane aperture domains. *Plant Cell* **30**, 2038–2056 (2018).
24. Chen, L. et al. Isolation and genetic analysis for rice mutants treated with ^{60}Co γ-ray. *J. Xiamen Univ.* **45**, 82–85 (2006).
25. Zhang, D. B. & Wilson, Z. A. Stamen specification and anther development in rice. *Chin. Sci. Bull.* **54**, 2342–2353 (2009).
26. Vaid, N., Macovei, A. & Tuteja, N. Knights in action: lectin receptor-like kinases in plant development and stress responses. *Mol. Plant.* **6**, 1405–1418 (2013).
27. Chen, C. et al. The lectin receptor kinase-VI.2 is required for priming and positively regulates *Arabidopsis* pattern-triggered immunity. *Plant Cell* **24**, 1256–1270 (2012).
28. Labbé, J. et al. Mediation of plant–mycorrhizal interaction by a lectin receptor-like kinase. *Nat. Plants* **5**, 676–680 (2019).
29. Wan, J. et al. A lectin receptor-like kinase is required for pollen development in *Arabidopsis*. *Plant Mol. Biol.* **67**, 469–482 (2008).
30. Shao, W. & Dong, J. Polarity in plant asymmetric cell division: Division orientation and cell fate differentiation. *Dev. Biol.* **419**, 121–131 (2016).
31. Zhang, Y., Guo, X. & Dong, J. Phosphorylation of the polarity protein BASL differentiates asymmetric cell fate through MAPKs and SPCH. *Curr. Biol.* **176**, 139–148 (2017).
32. Bellande, K., Bono, J. J., Savelli, B., Jamet, E. & Canut, H. Plant lectins and lectin receptor-like kinases: how do they sense the outside? *Int. J. Mol. Sci.* **18**, 1164 (2017).
33. Peng, X. et al. Lectin receptor kinase OsLecRK-S.7 is required for pollen development and male fertility. *J. Int. Plant Biol.* https://doi.org/10.1111/jipb.12897 (2020).
34. Liu, H. et al. Genetic analysis and mapping of rice (*Oryza sativa* L.) male-sterile (*OsMS-L*) mutant. *Chin. Sci. Bull.* **50**, 122–125 (2005).
35. Li, N. et al. The rice *Tapetum Degeneration Retardation* gene is required for tapetum degradation and anther development. *Plant Cell* **18**, 2999–3014 (2006).
36. Liu, L. et al. Receptor-like kinase RUPO interacts with potassium transporters to regulate pollen tube growth and integrity in rice. *PLoS Genet.* **12**, 1–23 (2016).
37. Wang, C. et al. Resolvase OsGEN1 mediates DNA repair by homologous recombination. *Plant Physiol.* **173**, 1316–1329 (2017).
38. Zhang, H. et al. Carbon starved anther encodes a MYB domain protein that regulates sugar partitioning required for rice pollen development. *Plant Cell* **22**, 672–689 (2010).
39. Hu, B. et al. Nitrate–NRT1.1B–SPX4 cascade integrates nitrogen and phosphorus signalling networks in plants. *Nat. Plants* **5**, 401–413 (2019).

Acknowledgements

This work was supported by grants from the National Key Research and Development Program of China (2016YFD0100902), the National Transgenic Major Program Grant (2016ZX08009-003), National Natural Science Foundation of China (31670309), the Innovative Research Team, Ministry of Education, and 111 Project (Grant B14016).

Author contributions

W.L. and D.Z. designed the project. X.Z. and G.Z. performed most of the experiments. H.Y. performed the map-based cloning. Q.T. performed the rice transformation. L.Z. and Q.T. performed the TEM sections. W.L., X.Z. and N.B. wrote the paper.

Competing interests

The authors declare no competing interests.

Additional information

Extended data is available for this paper at https://doi.org/10.1038/s41477-020-0630-6.

Supplementary information is available for this paper at https://doi.org/10.1038/s41477-020-0630-6.

Correspondence and requests for materials should be addressed to W.L.

Peer review information *Nature Plants* thanks Anna Dobritsa, Dazhong Zhao and the other, anonymous, reviewers for their contribution to the peer review of this work.

Reprints and permissions information is available at www.nature.com/reprints.

Publisher's note Springer Nature remains neutral with regard to jurisdictional claims in published maps and institutional affiliations.

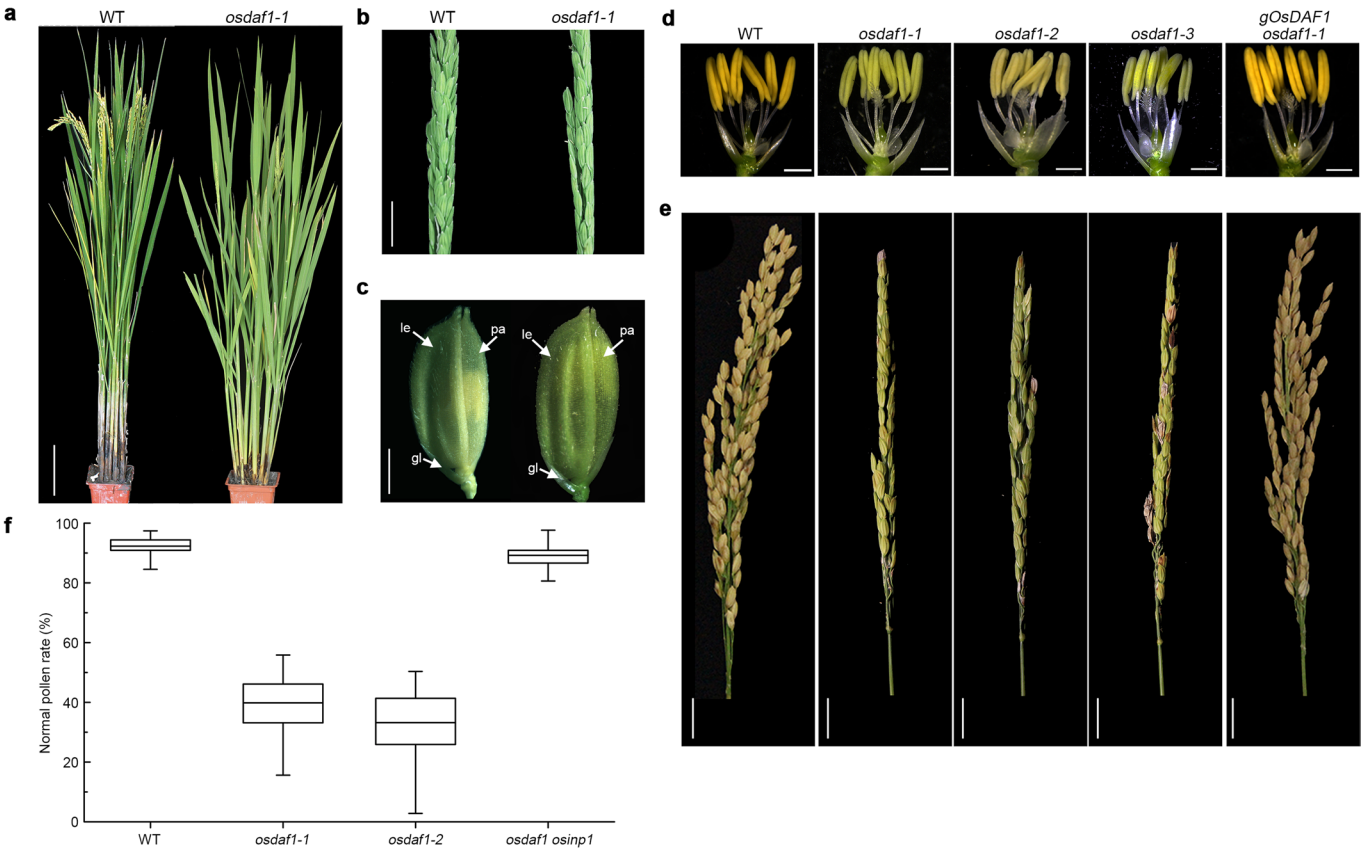

Extended Data Fig. 1 | Phenotypes and complementation of *osdaf1* mutants. a–c, Comparisons of wild type (WT) and *osdaf1-1* mature plants (**a**), flowering panicles (**b**) and spikelets (**c**). le, lemma; pa; palea; gl, glume. **d**, **e**, Comparisons of WT, *osdaf1-1*, *osdaf1-2*, *osdaf1-3* and *gOsDAF1 osdaf1-1* flowers (**d**) and mature panicles (**e**). **f**, The proportion of viable pollen produced by wild-type and mutant plants displayed as box plots, showing the first and third quartiles, split by the median and extended to minimum and maximum values. For each line, 50 independent replicates, each of at least 100 pollen grains, were counted. The phenotypes in **a**–**e** were observed at least three times independently with similar results. Scale bars, 10 cm (**a**), 1 cm (**b**, **e**) and 1 mm (**c**, **d**).

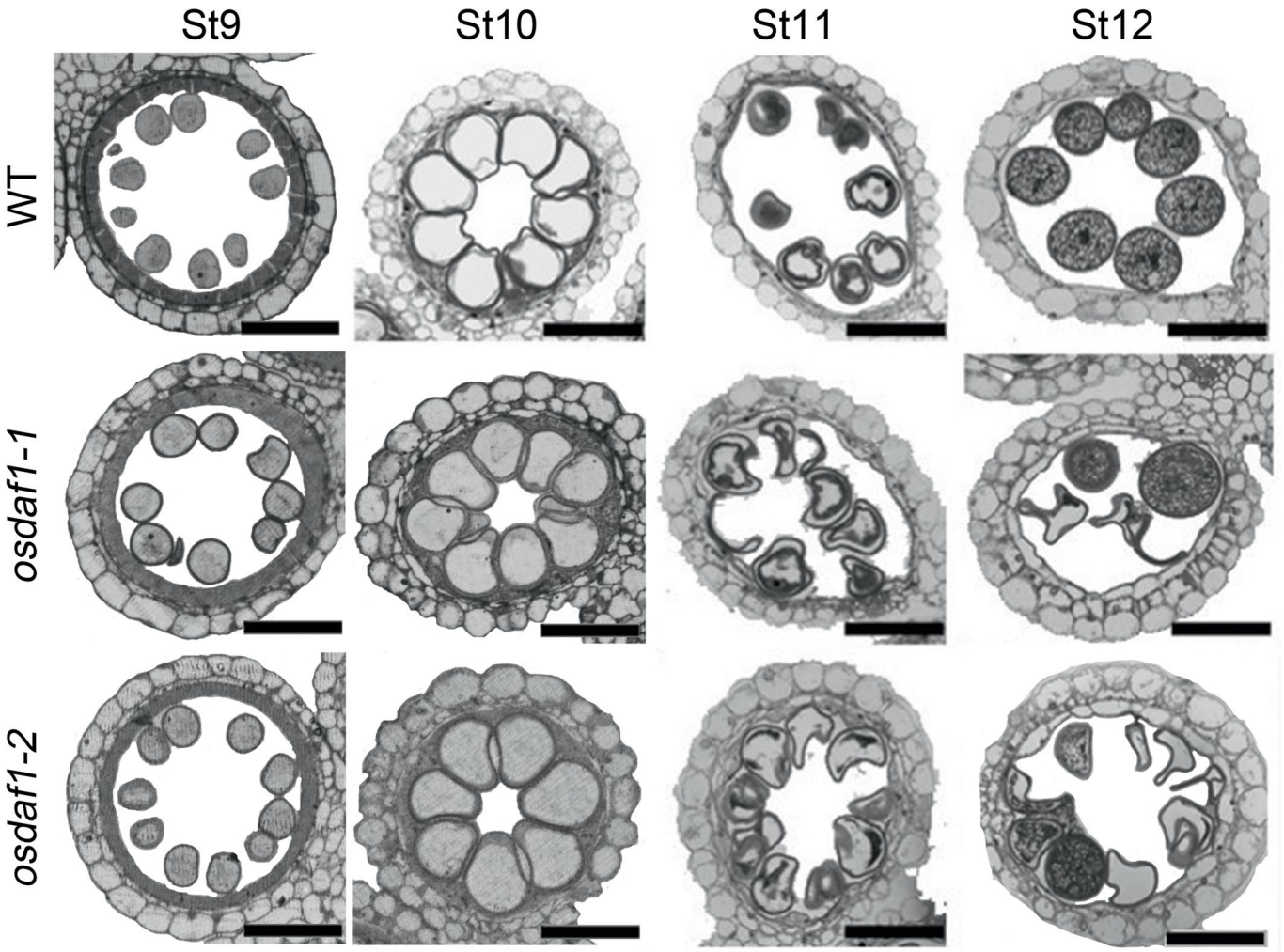

Extended Data Fig. 2 | Anther transverse sections of wild-type and *osdaf1* plants. Transverse sections of wild-type, *osdaf1-1* and *osdaf1-2* anthers at different developmental stages. Phenotypes were observed three times independently with similar results. Scale bars, 80 μm.

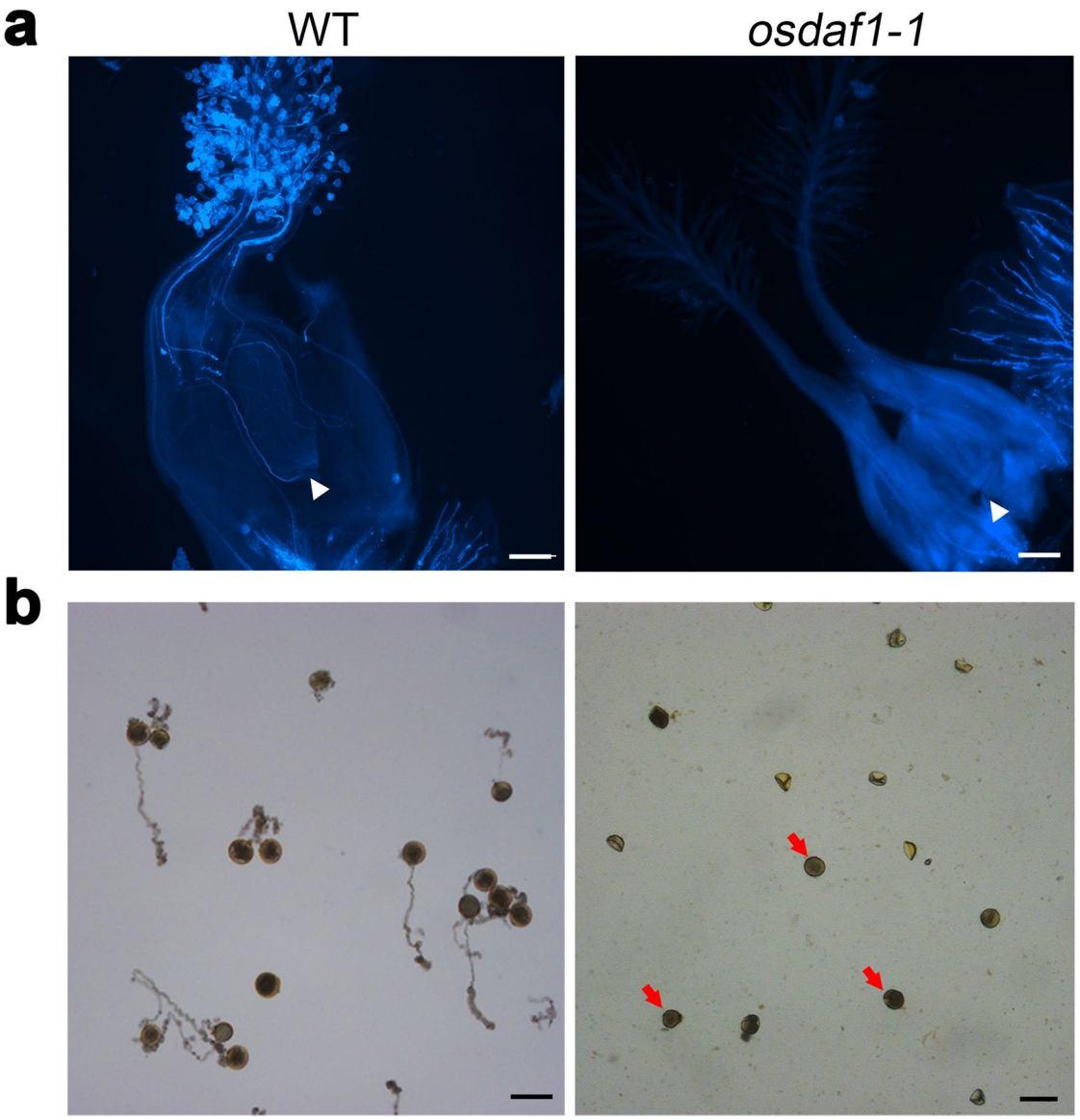

Extended Data Fig. 3 | Pollen germination assay of wild-type and *osdaf1* plants. *In vivo* (**a**) and *in vitro* (**b**) pollen germination assays of wild-type and *osdaf1-1* pollen grains. Arrowheads in **a** indicate the ovule; arrows in **b** indicate mutant pollen grains that failed to germinate. These experiments were repeated three times independently with similar results. Scale bars, 200 μm (**a**) and 50 μm (**b**).

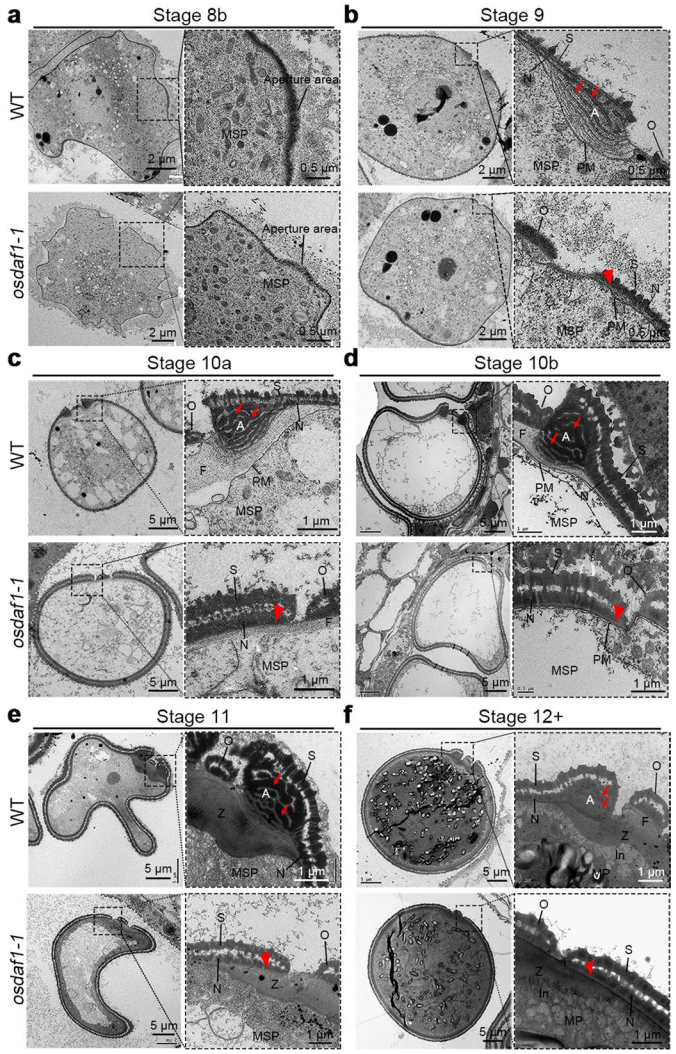

Extended Data Fig. 4 | TEM observation of wild-type and *osdaf1-1* pollen aperture areas. Microspores (left panel) and enlarged aperture areas (right panel) from wild-type (upper panel) and *osdaf1-1* (lower panel) at stage 8b (**a**), stage 9 (**b**), stage 10a (**c**), stage 10b (**d**), stage 11 (**e**), and stage 12 (**f**). A, annulus; N, nexine; S, sexine; O, operculum; PM, plasma membrane; MSP, microspore; MP, mature pollen; F, fibrillar-granular layer; Z, Zwischenkörper layer; In, intine. Arrows indicate the trilamellated structures in annulus. Arrowheads indicate the missing annulus structure in *osdaf1-1* pollen. These phenotypes were observed three times independently with similar results. Scale bars are indicated.

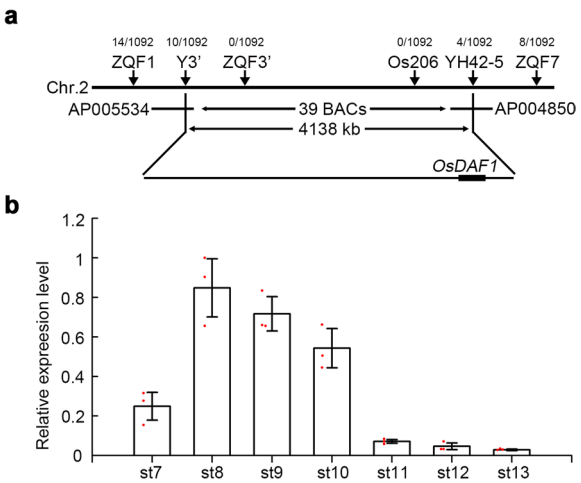

Extended Data Fig. 5 | Identification of *OsDAF1*. a, Fine mapping of *OsDAF1*. Positions and numbers of recombinants of each molecular marker are indicated. The *OsDAF1* locus is mapped to a 4138 kb region between Y3′ and YH42-5. AP005534 and AP004850 are accession numbers of BAC clones containing the two molecular markers. **b**, qRT-PCR analysis of *OsDAF1*. Quantification was normalized to the expression of the internal control *ACTIN*. n = 3 biologically independent samples of 50 μg anther from each stage. Data are mean ± SD; dots show data distribution.

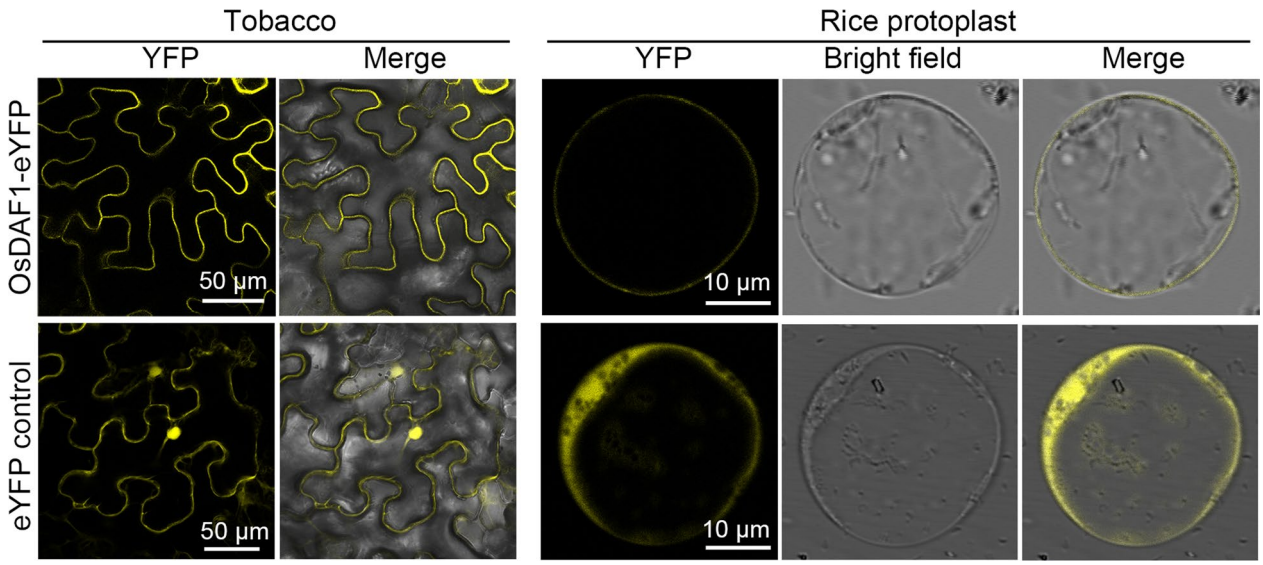

Extended Data Fig. 6 | Subcellular localizations of OsDAF1. Subcellular localizations of OsDAF1-eYFP protein in tobacco leaf epidermal cells (left panel) and rice protoplasts (right panel). The subcellular localizations were observed three times independently with similar results. Scale bars are indicated.

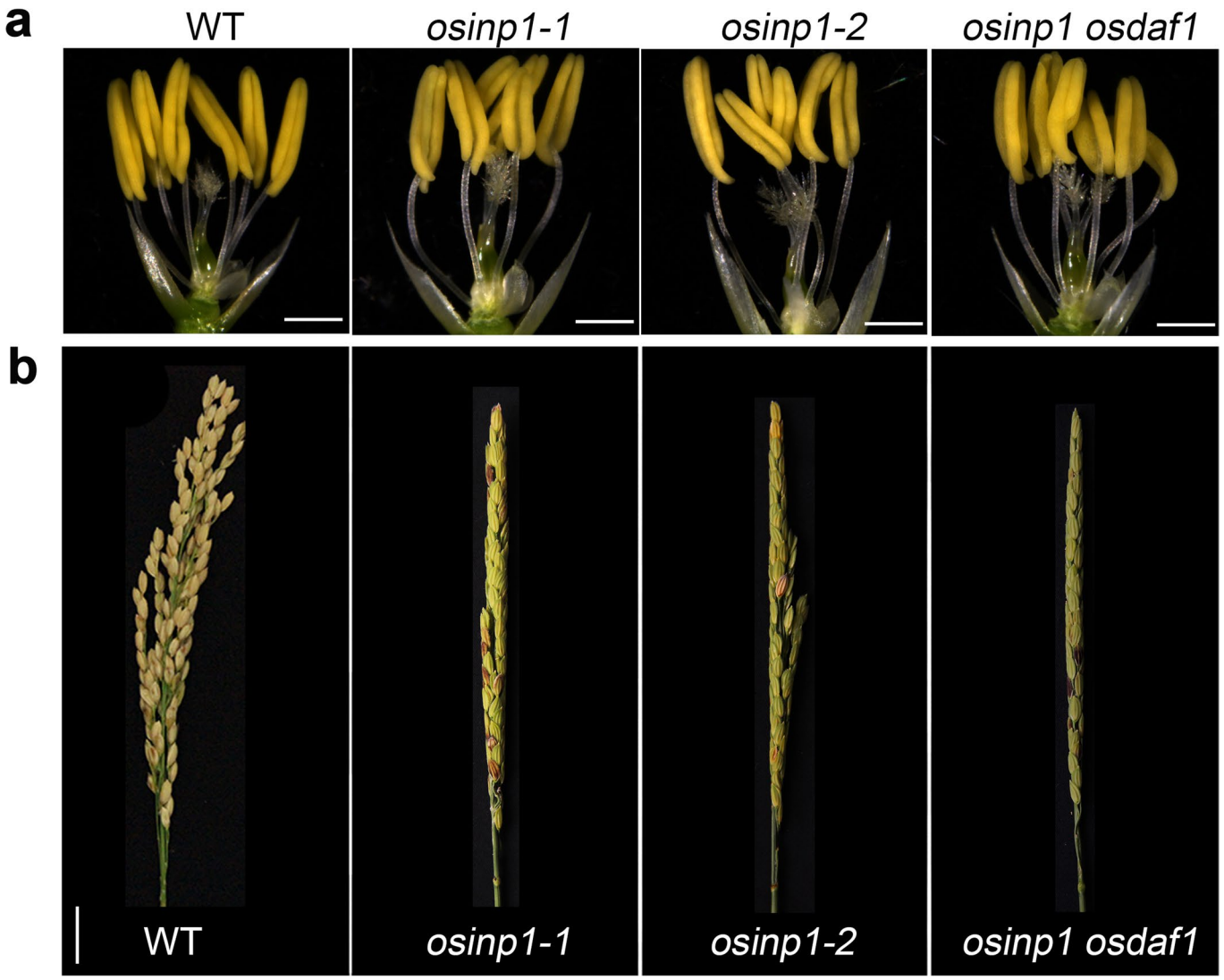

Extended Data Fig. 7 | Phenotypes of *osinp1* mutants. a, Comparisons of WT, *osinp1-1*, *osinp1-2* and *osinp1 osdaf1* flowers (**a**) and mature panicles (**b**). These phenotypes were observed at least three times independently with similar results. Scale bars, 1 mm (**a**) and 1 cm (**b**).

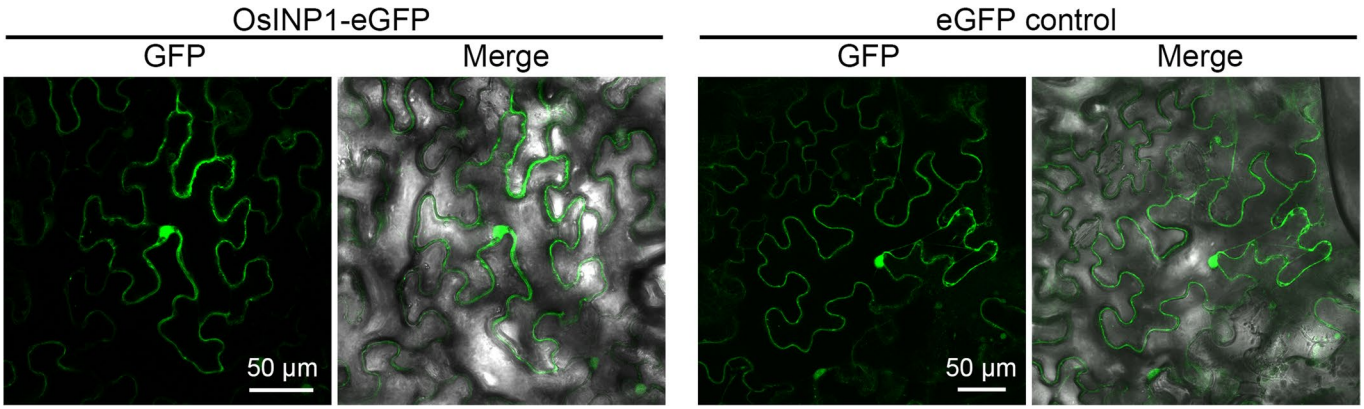

Extended Data Fig. 8 | Subcellular localization of OsINP1. Subcellular localization of OsINP1-eGFP in tobacco leaf epidermal cells. This subcellular localization was observed three times independently with similar results. Scale bars are indicated.

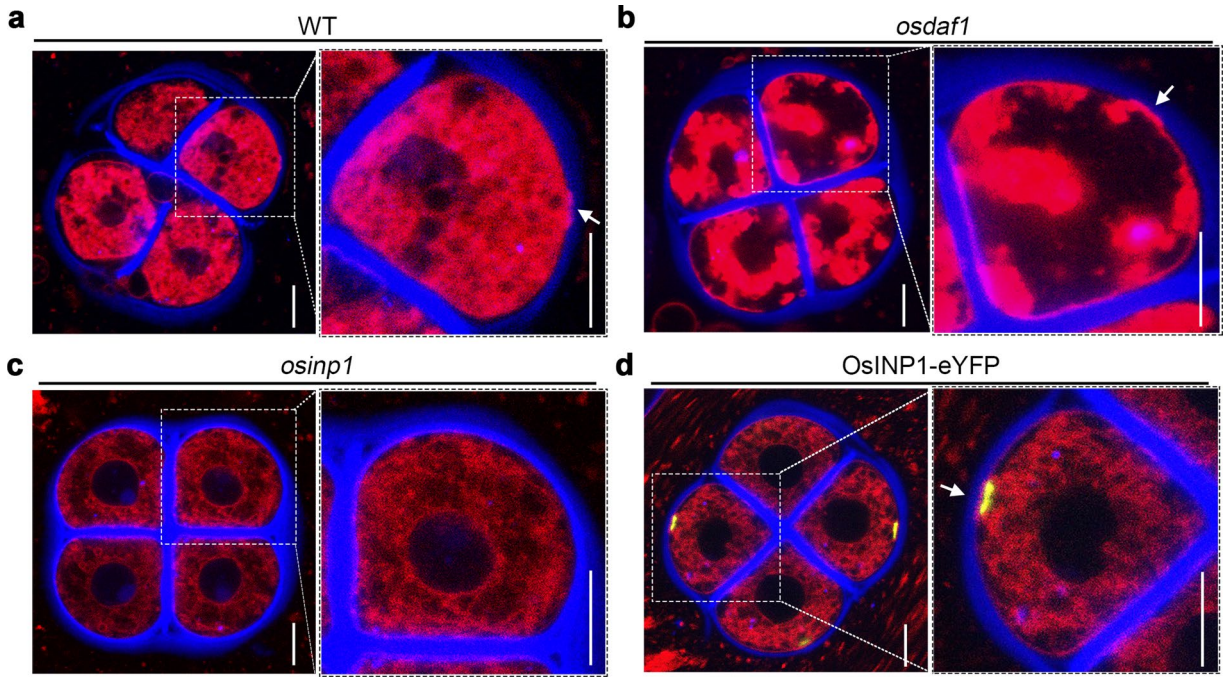

Extended Data Fig. 9 | OsINP1 modifies plasma membrane at aperture sites. Confocal images of tetrads stained by Calcofluor White (blue, callose wall) and CellMask Deep Red (red, membranous structures) from WT (**a**), *osdaf1* (**b**), *osinp1* (**c**) and OsINP1-eYFP transgenic plants (**d**). Merged fluorescent signal from YFP (yellow), Calcofluor White and CellMask Deep Red were shown in **d**. Arrows indicate the protruded membrane regions. These observations were repeated at least three times independently with similar results. Scale bars, 5 μm.

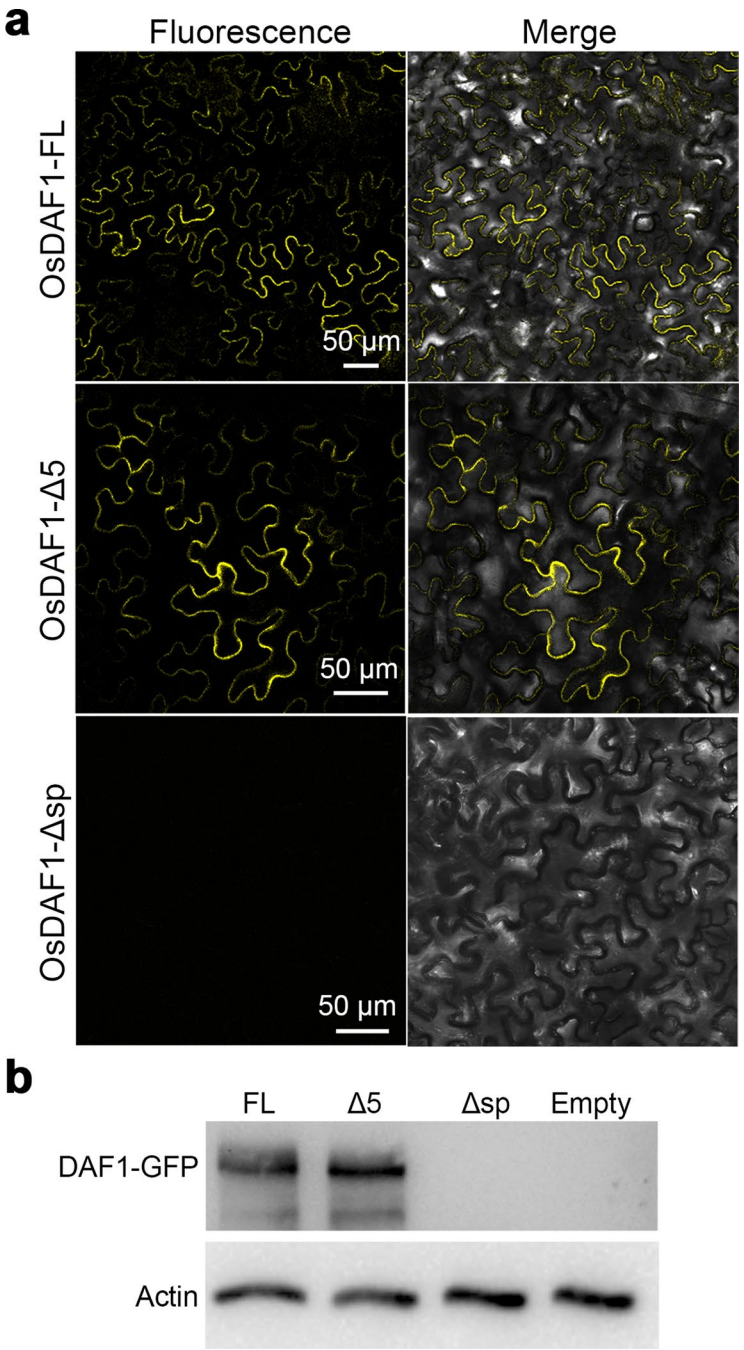

Extended Data Fig. 10 | Signal peptide of OsDAF1 may be essential for protein stability. a, Expression of full length OsDAF1 (upper panel), 5 amino acid truncated OsDAF1-GFP (middle panel, described in Fig. 5a) or signal peptide truncated OsDAF1-eYFP (lower panel) in tobacco leaf epidermal cells. **b**, The protein level of full length or truncated OsDAF1 in indicated samples, as determined by western blot. "Empty" represents a tobacco sample without Agrobacterium infiltration. Observations and data were repeated three times independently with similar results. Scale bars are indicated.

nature research

Corresponding author(s): Wan-Qi Liang

Last updated by author(s): Feb 20, 2020

Reporting Summary

Nature Research wishes to improve the reproducibility of the work that we publish. This form provides structure for consistency and transparency in reporting. For further information on Nature Research policies, see Authors & Referees and the Editorial Policy Checklist.

Statistics

For all statistical analyses, confirm that the following items are present in the figure legend, table legend, main text, or Methods section.

n/a	Confirmed
☐	☒ The exact sample size (*n*) for each experimental group/condition, given as a discrete number and unit of measurement
☐	☒ A statement on whether measurements were taken from distinct samples or whether the same sample was measured repeatedly
☐	☒ The statistical test(s) used AND whether they are one- or two-sided *Only common tests should be described solely by name; describe more complex techniques in the Methods section.*
☒	☐ A description of all covariates tested
☒	☐ A description of any assumptions or corrections, such as tests of normality and adjustment for multiple comparisons
☐	☒ A full description of the statistical parameters including central tendency (e.g. means) or other basic estimates (e.g. regression coefficient) AND variation (e.g. standard deviation) or associated estimates of uncertainty (e.g. confidence intervals)
☒	☐ For null hypothesis testing, the test statistic (e.g. *F*, *t*, *r*) with confidence intervals, effect sizes, degrees of freedom and *P* value noted *Give P values as exact values whenever suitable.*
☒	☐ For Bayesian analysis, information on the choice of priors and Markov chain Monte Carlo settings
☒	☐ For hierarchical and complex designs, identification of the appropriate level for tests and full reporting of outcomes
☒	☐ Estimates of effect sizes (e.g. Cohen's *d*, Pearson's *r*), indicating how they were calculated

Our web collection on statistics for biologists contains articles on many of the points above.

Software and code

Policy information about availability of computer code

Data collection	For bioinfomatic analysis, BLAST search of OsDAF1 was conducted on NCBI website (http://www.ncbi.nlm.nih.gov/). For confocal imaging, LAS X software was used to obtain figures.
Data analysis	The percent of identity of OsDAF1 homologs were based on BLAST results from NCBI. Box plot and histogram was produce using Origin9 software.

For manuscripts utilizing custom algorithms or software that are central to the research but not yet described in published literature, software must be made available to editors/reviewers. We strongly encourage code deposition in a community repository (e.g. GitHub). See the Nature Research guidelines for submitting code & software for further information.

Data

Policy information about availability of data

All manuscripts must include a data availability statement. This statement should provide the following information, where applicable:

- Accession codes, unique identifiers, or web links for publicly available datasets
- A list of figures that have associated raw data
- A description of any restrictions on data availability

All data supporting the findings of this study are available within the article and its Supplementary Information files or from the corresponding author upon reasonable request.

Field-specific reporting

Please select the one below that is the best fit for your research. If you are not sure, read the appropriate sections before making your selection.

☒ Life sciences ☐ Behavioural & social sciences ☐ Ecological, evolutionary & environmental sciences

For a reference copy of the document with all sections, see nature.com/documents/nr-reporting-summary-flat.pdf

Life sciences study design

All studies must disclose on these points even when the disclosure is negative.

Sample size	For qRT experiment, 50 μg anther samples of each stage was used to extract RNA. For co-ip and western blot assay, 500 μg of tobacco powder was used to extract total protein.
Data exclusions	No data was excluded
Replication	Every experiment was repeated for at least three times, and similar results were obtained.
Randomization	Sample allocation is not relevant to our study. Comparison of phenotypes was based on different genotypes. Blinding
Blinding	All the experiments were performed without prior knowledge of the final outcome, and therefore blinding was not applied.

Reporting for specific materials, systems and methods

We require information from authors about some types of materials, experimental systems and methods used in many studies. Here, indicate whether each material, system or method listed is relevant to your study. If you are not sure if a list item applies to your research, read the appropriate section before selecting a response.

Materials & experimental systems

n/a	Involved in the study
☐	☒ Antibodies
☒	☐ Eukaryotic cell lines
☒	☐ Palaeontology
☒	☐ Animals and other organisms
☒	☐ Human research participants
☒	☐ Clinical data

Methods

n/a	Involved in the study
☒	☐ ChIP-seq
☒	☐ Flow cytometry
☒	☐ MRI-based neuroimaging

Antibodies

Antibodies used	Commercial antibodies used: α-GFP (G1544, Rabbit polyclonal antibody, Sigma, 1:5000 dilution), α-HA (M20003, Mouse monoclonal antibody, Abmart, 1:2000 dilution), α-actin (M20009, Mouse monoclonal antibody, Abmart, 1:2000 dilution), Goat Anti-Mouse IgG HRP (M21001, Abmart, 1:5000 dilution), Goat Anti-Rabbit IgG HRP (M21002, Abmart, 1:5000 dilution).
Validation	Anti-GFP, anti-HA, anti-actin, goat anti-mouse IgG-HRP and goat anti-rabbit IgG-HRP antibodies are commercially available and validated by Western blotting and/or in prior publications on the following websites. Anti-GFP: https://www.sigmaaldrich.com/catalog/product/sigma/g1544?lang=zh&region=CN; Anti-HA: http://www.ab-mart.com.cn/page.aspx?node=60&id=963 Anti-Actin: http://www.ab-mart.com.cn/page.aspx?node=59&id=985 Goat anti-mouse IgG-HRP: http://www.ab-mart.com.cn/page.aspx?node=62&id=960 Goat anti-rabbit IgG-HRP: http://www.ab-mart.com.cn/page.aspx?node=62&id=980